

Structure-Based Design and Optimization of Multitarget-Directed 2H-Chromen-2-one Derivatives as Potent Inhibitors of Monoamine Oxidase B and Cholinesterases

Roberta Farina,[†] Leonardo Pisani,[†] Marco Catto,^{*,†} Orazio Nicolotti,[†] Domenico Gadaleta,[†] Nunzio Denora,[†] Ramon Soto-Otero,[‡] Estefania Mendez-Alvarez,[‡] Carolina S. Passos,[§] Giovanni Muncipinto,^{†,||} Cosimo D. Altomare,[†] Alessandra Nurisso,[§] Pierre-Alain Carrupt,[§] and Angelo Carotti^{*,†}

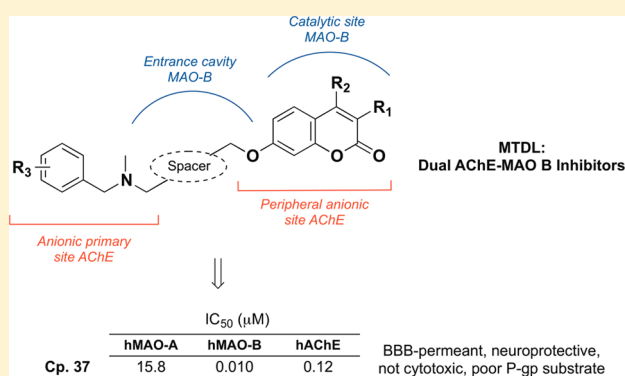
[†]Dipartimento di Farmacia—Scienze del Farmaco, Università degli Studi di Bari “Aldo Moro”, Via E. Orabona 4, I-70125 Bari, Italy

[‡]Grupo de Neuroquímica, Departamento de Bioquímica y Biología Molecular, Facultad de Medicina, Universidad de Santiago de Compostela, San Francisco I, E-15782, Santiago de Compostela, Spain

[§]School of Pharmaceutical Sciences, University of Geneva, University of Lausanne, Quai Ernest Ansermet 30, CH-1211, Geneva 4, Switzerland

Supporting Information

ABSTRACT: The multifactorial nature of Alzheimer’s disease calls for the development of multitarget agents addressing key pathogenic processes. To this end, by following a docking-assisted hybridization strategy, a number of aminocoumarins were designed, prepared, and tested as monoamine oxidases (MAOs) and acetyl- and butyryl-cholinesterase (AChE and BChE) inhibitors. Highly flexible *N*-benzyl-*N*-alkoxy coumarins 2–12 showed good inhibitory activities at MAO-B, AChE, and BChE but low selectivity. More rigid inhibitors, bearing *meta*- and *para*-xylyl linkers, displayed good inhibitory activities and high MAO-B selectivity. Compounds 21, 24, 31, 37, and 39, the last two featuring an improved hydrophilic/lipophilic balance, exhibited excellent activity profiles with nanomolar inhibitory potency toward hMAO-B, high hMAO-B over hMAO-A selectivity and submicromolar potency at hAChE. Cell-based assays of BBB permeation, neurotoxicity, and neuroprotection supported the potential of compound 37 as a BBB-permeant neuroprotective agent against H₂O₂-induced oxidative stress with poor interaction as P-gp substrate and very low cytotoxicity.



INTRODUCTION

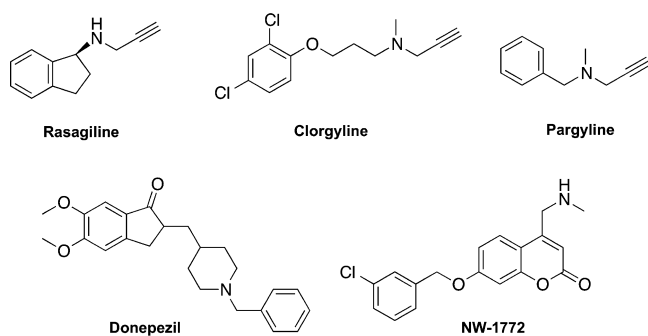
Neurodegenerative diseases (NDs) are widely investigated pathologies because of the low efficacy of current therapies^{1,2} and severe functional impairments for daily life activities, resulting in high familiar, social, and financial costs of patient care.³ Despite the huge efforts in private and public research settings, most clinical trials of potential drug candidates for NDs, and for Alzheimer’s disease (AD) in particular,^{4,5} failed. As a result, valuable disease-modifying therapies for NDs are still missing.

AD and Parkinson’s disease (PD) are the most widespread and severe NDs. AD is the result of a progressive loss of neurons in basal forebrain regions associated with abnormal accumulation of beta amyloid protein (Aβ) in neuronal plaques and hyperphosphorylated tau protein in neurofibrillary tangles.⁶ Neuronal degeneration in AD is triggered and maintained by low molecular weight Aβ oligomers and by reactive oxygen species (ROS), produced by oxidative degradation of neuro-

transmitters and xenobiotics.⁷ The brain regions mostly affected by neuronal loss are essentially made of cholinergic neurons, so that restoring physiological acetylcholine levels has been considered a viable therapy in AD, as claimed by the so-called *cholinergic hypothesis*.⁸ To date, drugs approved for AD therapy are the cholinesterase (ChE) inhibitors rivastigmine, galantamine, and donepezil^{9,10} (Chart 1). The NMDA partial antagonist memantine has also been approved for the symptomatic treatment of AD for its contrasting effects over glutamate excitotoxicity.¹¹

Acetylcholinesterase (AChE, EC 3.1.1.7), the key enzyme targeted in the palliative therapy of AD, is present in both central and peripheral nervous system and in muscular motor plaques and is responsible for the enzymatic cleavage of neurotransmitter acetylcholine (ACh). The other ChE, 63

Received: April 17, 2015

Chart 1. Chemical Structures of Reference AChE and MAO Inhibitors

64 butyrylcholinesterase (BChE, EC 3.1.1.8), present in brain and
65 peripheral tissues, but prevalently in serum, is up-regulated in
66 advanced AD and may play a role in the maintenance and
67 progression of the disease.¹²

68 The catalytic cleavage of ACh involves a tight cooperation of
69 three amino acids, the so-called catalytic triad (Ser-His-Glu)
70 and aromatic amino acid residues responsible for cation- π
71 interactions.¹³ The catalytic bottom cleft represents one of the
72 binding sites for substrates and inhibitors, along with the
73 peripheral anionic binding site constituted by a larger region
74 lined chiefly by aromatic amino acids. This structural
75 arrangement accounts for the strong binding interactions
76 observed for inhibitors such as decamethonium and donepezil,
77 able to interact with both catalytic (CAS) and peripheral (PAS)
78 anionic binding sites of AChE and, therefore, called dual
79 binding site (DBS) inhibitors.¹⁴ As binding interactions at the
80 PAS reduces the aggregation of A β peptide(s) leading to
81 amyloid oligomers, DBS inhibitors are endowed with dual
82 inhibitory activity on AChE and A β aggregation.¹⁵

83 The availability of X-ray crystallographic coordinates of many
84 AChE-inhibitor complexes has allowed the identification of
85 key interactions for high ligand binding affinity¹⁶ and has
86 enabled the target-based design of potent and selective AChE
87 inhibitors (AChEIs). In this context, potent AChE inhibition by
88 coumarin derivatives,^{17,18} homo- and heterobis-quaternary
89 ammonium salts,^{19,20} 2-quinolones,²¹ and other heterocyclic
90 compounds²²⁻²⁴ have been reported by our group.

91 In the therapy of PD, a key target enzyme is represented by
92 monoamine oxidase (MAO; amine-oxygen oxidoreductase, EC
93 1.4.3.4), a FAD-dependent enzyme, responsible for oxidative
94 deamination of amine neurotransmitters, including dopamine
95 that is depleted in PD, and exogenous amines.^{25,26} Two
96 isoforms of MAO, namely MAO-A and MAO-B, have been
97 characterized in terms of amino acid sequence, tissue
98 distribution, and selectivity toward substrates and inhibi-
99 tors.^{27,28} Selective MAO-A inhibitors (MAO-AIs: e.g., clorgy-
100 line and moclobemide) are used in the treatment of depression,
101 while selective MAO-BIs, i.e., rasagiline and selegiline, are
102 employed as adjuvant or alternative drugs to L-DOPA in PD
103 therapy.^{29,30}

104 The resolution of the X-ray crystal structures of both human
105 MAO-A^{31,32} and MAO-B³³⁻³⁵ bound to several inhibitors has
106 newly spurred the research in the field of MAO inhibition,
107 given to its therapeutic potential in neurological disorders,
108 including AD, where selective MAO-BIs may play a role.^{29,36}

109 Growing evidence in the past few years has outlined the
110 multifactorial etiopathogenesis of AD, PD, and other NDs.
111 Actually, neurodegeneration is a complex pathological event

112 resulting from the imbalance and deregulation of multiple
113 biochemical pathways, ultimately depending on transcriptional
114 and epigenetic modulations and on environmental factors.³⁷ As
115 a consequence, holistic, multifaceted pathologies are currently
116 tackled by a polypharmacological approach based on multi-
117 targeted therapy.^{29,38,39} The paradigm “one drug—one target”
118 has nowadays evolved into a more challenging “one drug—more
119 targets” approach, provided that a good balance among
120 potencies and efficacy toward selected targets, and optimal
121 ADME-T properties, can be achieved.⁴⁰⁻⁴²

122 ■ MULTITARGET-LIGAND DESIGN: RATIONALE AND 123 METHODS

124 The experience achieved by our group in the field of ligand-
125 and target-based design of potent, selective, and reversible
126 MAO⁴³⁻⁵⁰ and ChE inhibitors,¹⁷⁻²⁴ prompted us to further
127 explore the challenging field of multitargeted ligand design by
128 addressing compounds with dual MAO and AChE inhibition.
129 The earliest application of this approach by us was reported
130 nearly 15 years ago, when we discovered coumarin derivatives
131 endowed with good and moderate inhibition against MAO-B
132 and AChE, respectively.⁵¹ Additional data have been later
133 presented in an international meeting.⁵²

134 Since then, many authors have described the potential
135 therapeutic application of multimodal MAO-Is displaying
136 additional activities, such as AChE inhibition,⁵³⁻⁵⁹ metal ion
137 chelation,⁶⁰ antioxidant,^{61,62} and neuroprotective activities.⁶³
138 Further studies suggested the combination of MAO and ChE
139 inhibition in the same molecule as a promising strategy in the
140 treatment of AD.⁶⁴

141 Starting from our previous findings,⁵¹ we designed,
142 synthesized, and tested a new series of suitably substituted
143 coumarin derivatives with the aim of discovering multipotent
144 compounds with different bioactivity profiles toward MAO-B
145 and AChE. While MAO-B selectivity was an important goal of
146 our study to avoid unwanted side effects arising from the
147 intestinal MAO-A inhibition and the consequent hypertensive
148 effect coming from tyramine-rich food (tyramine is indeed
149 metabolized by intestinal MAO-A),⁶⁵ the lack of AChE over
150 BChE selectivity was not deemed as important⁶⁶ due to a likely
151 pathogenic role of BChE in advanced AD.⁶⁷

152 The molecular framework of our new multitarget ligands was
153 built following a hybridization strategy. Starting from known
154 ligands of the two enzymes, simple pharmacophore motifs were
155 selected and joined in a unique molecular entity. As molecular
156 flexibility plays a key role in accommodating ligands inside the
157 AChE narrow gorge, a small series of hybrids was designed by
158 connecting the coumarin core of 7-(3-chlorobenzoyloxy)-3-
159 methylcoumarin (MC 1095)⁴⁵ to the *N*-benzylaminomethyl
160 group characterizing many AChE inhibitors (e.g., donepezil)
161 through a flexible spacer (Figure 1). The 2*H*-chromen-2-one
162 ring of such compound was chosen as the moiety able to
163 efficiently fit the MAO-B enzymatic cleft by facing the
164 isoalloxazine ring of FAD. In the additional series of more
165 rigid hybrids, to improve AChE inhibitory potency of 7-
166 benzyloxycoumarins,⁴⁴ we approached a “designing in”
167 strategy^{29,39,42} by adding in a suitable position of the coumarin
168 ring a protonatable basic moiety that might bind CAS through
169 π -cation interactions (Figure 2). Taking into account that, as
170 recently reported,^{68,69} the steric hindrance of substituents
171 placed at position 4 of the coumarin ring exerts a negative
172 impact on MAO affinity, the basic head was anchored to the 7-
173 benzyloxy substituent. This rational hybrid design was

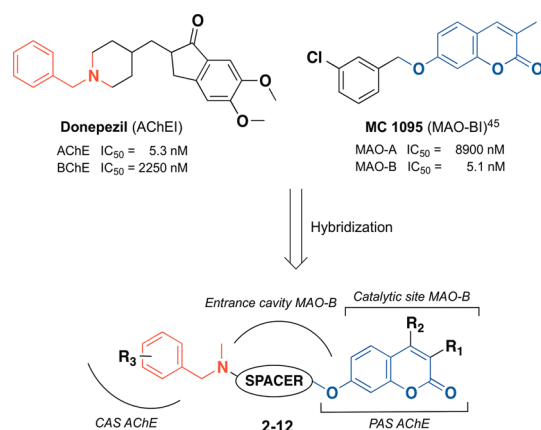


Figure 1. Hybridization strategy for flexible multitarget MAO-B/AChE inhibitors **2–12**.

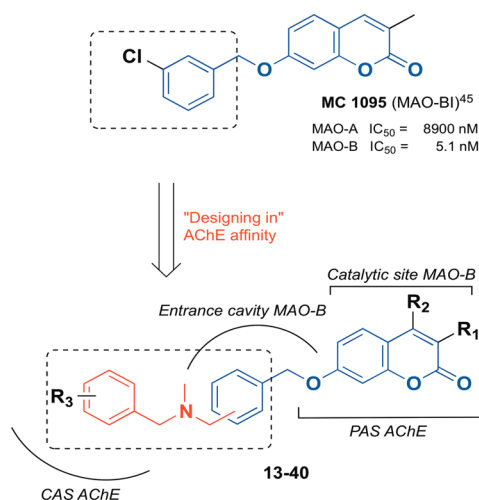


Figure 2. Hybridization strategy for rigid molecules as multitarget MAO-B/AChE inhibitors **13–40**.

supported by prospective docking studies based on X-ray 174
crystal structures of the two target enzymes. As suggested by 175
docking calculations, the protonatable head may establish π - 176
cation interactions at the CAS of AChE, while the coumarin 177
moiety may interact with PAS.¹⁷ Such a pose resembled that of 178
donepezil in the PDB complexes (entries: 1EVE and 4EY7). As 179
for the binding to MAO-B, docking studies revealed that the 180
coumarin nucleus can be accommodated in the catalytic region 181
in proximity of FAD, thus matching the pose experimentally 182
observed in the X-ray crystal structure of MAO-B selective 183
coumarin inhibitor NW-1772 (Chart 1).⁴⁹ The spacer tethering 184
the two main pharmacophore features, namely the coumarin 185
nucleus and the protonatable amine moiety, was examined also 186
in terms of a reduced flexibility, by synthesizing the *meta*- and 187
para-xylyl derivatives listed in Table 2, to determine the optimal 188 t112
distance between the two key binding moieties in both target 189
enzymes. 190

Docking studies suggested that both polymethylene and xylyl 191
linkers overlaid, at least in part, with the 7-benzyloxy group of 192
NW-1772 that faces the MAO-B entrance cavity (acting as B/A 193
structural determinants for selectivity) and keeps the basic 194
moiety close to the aromatic region more proximal to the 195
solvent. 196

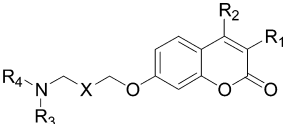
The newly synthesized coumarin derivatives **2–40**, **42**, and 197
43 were tested *in vitro* for their inhibition of rat MAO-A and 198
MAO-B (rMAOs), electric eel AChE (eeAChE), and equine 199
serum BChE (esBChE). The quinolone isoster **45** was also 200
synthesized and tested, taking into account our previous 201
findings on AChE inhibitors,²¹ with the aim of retaining activity 202
toward the target enzymes while possibly improving the 203
pharmacokinetics properties (i.e., lowering lipophilicity and 204
increasing metabolic stability). The most potent inhibitors at 205
rMAO-B and eeAChE were also assayed on the human 206
isoforms of the two MAOs and ChEs. The inhibition data of 207
nonhuman and human enzymes are reported in Tables 1–3 208 t3
and 4, respectively. Finally, compound **37**, which showed 209 t4
outstanding activities on human enzymes together with well- 210

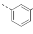
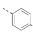
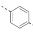
Table 1. MAO and ChE Inhibition Data of Coumarin Derivatives **2–12**

compd	X	R ₁	R ₂	IC ₅₀ , μ M (or inhibition % at 10 μ M)			
				MAO-A ^a	MAO-B ^a	AChE ^b	BChE ^c
2 ^d	–(CH ₂) ₃ –	Me	H	(35%)	0.33	1.3	7.8
3 ^d		Et	H	7.4	0.98	0.36	4.0
4	–(CH ₂) ₄ –	Me	H	6.6	1.1	0.49	3.7
5 ^d	–(CH ₂) ₅ –	H	H	2.2	0.50	0.94	1.8
6		Me	H	4.2	0.98	0.55	2.8
7 ^d		Me	3-CN	5.3	2.5	2.3	4.1
8 ^d		Me	3-Cl	(42%)	8.9	0.29	2.6
9 ^d		Me	4-CN	(48%)	3.3	2.8	4.3
10 ^d		Et	H	9.5	7.8	0.75	0.94
11	–(CH ₂) ₆ –	Me	H	0.51	1.7	0.095	0.67
12 ^d		Et	H	2.1	0.72	0.32	0.49

^aFrom rat brain. ^bFrom electric eel. ^cFrom equine serum. Values are mean of two/three independent experiments; SEM < 10%. ^dHydrochloride salt.

Table 2. MAO and ChE Inhibition Data of Coumarin Derivatives 13–40



compd	X	R ₁	R ₂	R ₃	R ₄	IC ₅₀ , μM (or inhibition % at 10 μM)			
						MAO-A ^a	MAO-B ^a	AChE ^b	BChE ^c
13		H	H	Me	Me	10	3.2	(38%)	5.3
14 ^d		H	H	Et	Et	(43%)	(35%)	1.7	6.8
15		H	H	Me	Bn	(8%)	2.0	2.3	1.0
16 ^d		H	H	Me	3-CNbn	(2%)	3.7	4.2	2.8
17 ^d		H	H	Me	3-MeOBn	(14%)	2.5	6.6	0.88
18 ^d		H	H	Me	3-ClBn	(17%)	3.4	5.7	0.31
19		H	H	Me	Me	(17%)	3.7	7.1	0.24
20		H	H	Et	Et	(9%)	(44%)	2.9	3.4
21		H	H	Me	Bn	(7%)	0.85	0.75	11
22 ^d		Me	H	Me	Bn	(0%)	2.4	0.26	1.1
23 ^d		H	Me	Me	Bn	(10%)	4.1	0.18	1.0
24 ^d		Me	Me	Me	Bn	(0%)	1.2	0.10	0.69
25 ^d		H	H	Me	3-CNbn	(5%)	2.8	7.4	4.1
26 ^d		H	H	Me	3-MeOBn	(20%)	2.9	4.6	1.4
27 ^d		H	H	Me	3-ClBn	(12%)	2.7	0.59	1.2
28 ^d		Me	H	Me	3-ClBn	(0%)	4.5	1.3	(29%)
29 ^d		H	Me	Me	3-ClBn	(0%)	5.0	0.12	(47%)
30 ^d		Me	Me	Me	3-ClBn	(7%)	3.4	0.66	(48%)
31 ^d		H	H	Me	4-CNbn	(6%)	0.27	5.6	4.4
32 ^d		Me	H	Me	4-CNbn	(15%)	1.7	7.0	(16%)
33 ^d		H	Me	Me	4-CNbn	(10%)	0.41	3.3	(29%)
34 ^d		Me	Me	Me	4-CNbn	(0%)	2.9	4.2	(18%)
35 ^d		CN	H	Me	Bn	(0%)	(41%)	0.20	5.5
36 ^d		CN	H	Me	4-CNbn	(0%)	0.99	(42%)	(14%)
37 ^d		H	CH ₂ OH	Me	Bn	(0%)	0.41	0.42	1.1
38		H	CH ₂ OH	H	Bn	(19%)	0.53	0.44	0.57
39 ^d		H	CH ₂ OH	Me	3-ClBn	(0%)	0.24	0.25	0.63
40 ^d		H	CH ₂ OH	Me	4-CNbn	(0%)	0.035	6.3	(23%)

^aFrom rat brain. ^bFrom electric eel. ^cFrom equine serum. Values are mean of two/three independent experiments; SEM < 10%. ^dHydrochloride salt.

CHEMISTRY

214

Compounds 2–40 were prepared from bromo-coumarin intermediates 1a–k through microwave-assisted reaction with appropriate benzylamines, in the presence of anhydrous potassium carbonate and a catalytic amount of potassium iodide, in anhydrous acetonitrile. Bromides 1a–k were, in turn, prepared from 7-hydroxycoumarin derivatives and commercial dibromides, as depicted in Scheme 1. Synthesis of analogues 42 and 43 (Scheme 2) started from the reduction of 4-(bromomethyl)phenylacetic acid with BH₃·SMe₂ complex to obtain alcohol 41a that was then coupled with 7-hydroxycoumarin. CBr₄/PPh₃-mediated bromination of 41b afforded 41c that underwent a final microwave-assisted nucleophilic substitution with the appropriate benzylamine, yielding the desired coumarins 42–43. As illustrated in Scheme 3, 7-hydroxy-2-quinolone 44b was prepared from the condensation of *trans*-cinnamic acid chloride with *m*-anisidine, followed by an intramolecular Friedel–Crafts acylation/dearylation⁷⁰ reaction in refluxing chlorobenzene in the presence of aluminum chloride as Lewis acid. Sequential regioselective alkylation of phenolic-OH with α,α' -dibromo-*p*-xylene and reaction of intermediate 44c with benzylmethylamine in the usual conditions gave final compound 45.

Analytical and spectroscopic data of tested compounds 2–40, 42, 43, and 45 are reported in Table 6 and Supporting Information.

BIOLOGICAL ASSAYS

240

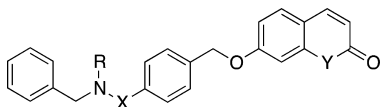
All compounds were tested for their inhibitory activities on rat MAOs (rMAOs), electric eel AChE (eeAChE), and equine serum BChE (esBChE) enzymes. For MAO inhibition test, the protocol using mitochondrial rMAO-A and -B obtained from rat brain homogenates was used as previously described.⁴⁵ As for eeAChE and esBChE, the well-known Ellman's spectrophotometric test⁷¹ was used to determine both IC₅₀s and inhibition kinetics. Results are reported in Tables 1–3 as IC₅₀ (μM) or, for poorly active compounds, as percentage of inhibition at 10 μM. Inhibition kinetics plots are depicted in Figure 3.

Compounds 2, 4, 5, 11, 12, 21–24, 29, 31–34, 37, 39, 40, and 45 were also tested on human isoenzymes of MAOs (hMAOs) and/or ChEs (hChEs). While hChEs were tested through the Ellman's method, the assays for hMAOs were carried out with a fluorescence-based method using kynuramine as a nonselective substrate of hMAO-A and hMAO-B.⁷² Results of inhibition tests on hMAOs and hChEs are reported in Table 4.

Apical to basolateral (AP-BL) and basolateral to apical (BL-AP) apparent permeability (P_{app}) of compound 37 was 260

balanced solubility/lipophilicity properties, was also investigated as potential CNS-permeant neuroprotective agent in vitro.

Table 3. Inhibition Data of Derivatives 42, 43, and 45



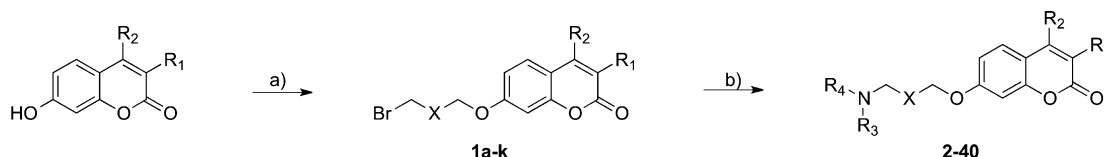
compd	R	X	Y	IC ₅₀ , μM (or inhibition % at 10 μM)			
				MAO-A ^a	MAO-B ^a	AChE ^b	BChE ^c
42 ^d	Me	–(CH ₂) ₂ –	O	(12%)	4.1	0.85	0.52
43 ^d	H	–(CH ₂) ₂ –	O	1.7	(45%)	4.7	0.64
45 ^d	Me	–CH ₂ –	NH	(10%)	(29%)	0.49	1.7

^aFrom rat brain. ^bFrom electric eel. ^cFrom equine serum. Values are mean of two/three independent experiments; SEM < 10%. ^dHydrochloride salt.

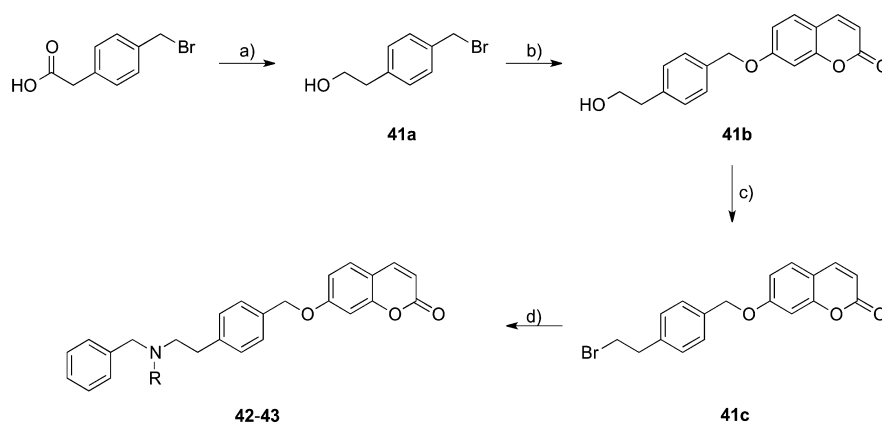
Table 4. Inhibition Data on hMAOs, hAChE, and hBChE

compd	IC ₅₀ μM (or inhibition % at 10 μM) ± SEM			
	hMAO-A ^a	hMAO-B ^a	hAChE ^b	hBChE ^c
2 ^d	(17 ± 6%)	0.134 ± 0.018	1.0 ± 0.1	nt
4	0.48 ± 0.04	0.096 ± 0.006	0.79 ± 0.01	nt
5 ^d	0.39 ± 0.05	0.029 ± 0.006	0.30 ± 0.01	0.95 ± 0.02
11	0.191 ± 0.053	0.321 ± 0.038	0.34 ± 0.03	0.95 ± 0.05
12 ^d	0.115 ± 0.015	0.018 ± 0.003	0.44 ± 0.06	nt
21	(0%)	0.041 ± 0.008	0.95 ± 0.08	0.89 ± 0.03
22 ^d	nt	nt	0.50 ± 0.03	nt
23 ^d	nt	nt	0.91 ± 0.07	nt
24 ^d	4.3 ± 0.1	0.053 ± 0.001	0.45 ± 0.03	(46 ± 4%)
29 ^d	nt	nt	1.0 ± 0.2	nt
31 ^d	(0%)	0.045 ± 0.013	6.0 ± 0.5	nt
32 ^d	(11 ± 3%)	0.017 ± 0.004	nt	nt
33 ^d	(39 ± 2%)	0.039 ± 0.001	8.5 ± 0.8	nt
34 ^d	(31 ± 4%)	0.024 ± 0.003	3.9 ± 0.5	nt
37 ^d	15.8 ± 2	0.010 ± 0.002	0.12 ± 0.01	9.3 ± 0.7
39 ^d	13.0 ± 2	0.024 ± 0.004	0.33 ± 0.03	(14 ± 3%)
40 ^d	4.48 ± 0.4	0.0057 ± 0.0008	nt	nt
45 ^d	(14 ± 3%) ^e	4.5 ± 0.2	1.5 ± 0.1	nt
Donepezil	(0%)	(0%)	0.015 ± 0.003	4.8 ± 0.6
Clorgyline	0.0049	11.0	nt	nt
Pargyline	4.10	0.13	nt	nt

^aHuman recombinant MAOs on Supersomes. ^bHuman recombinant AChE. ^cHuman serum BChE. ^dHydrochloride salt. ^eDetermined at 4 μM concentration. nt, not tested.

Scheme 1. Synthesis of Compounds 2–40^a

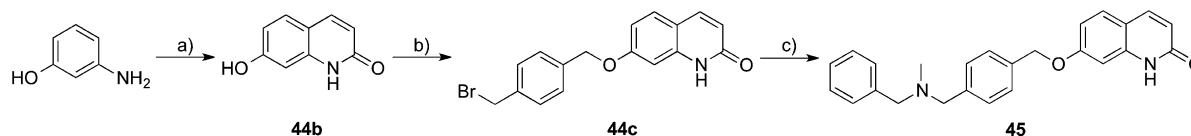
^aReagents and conditions: (a) suitable dibromo-derivative (1,3-dibromopropane for **1a**, 1,4-dibromobutane for **1b**, 1,5-dibromopentane for **1c**, 1,6-dibromohexane for **1d**, α,α' -dibromo-*m*-xylene for **1e**, α,α' -dibromo-*p*-xylene for **1f–k**), K₂CO₃, dry acetonitrile, 30 min, 130 °C, MW; (b) substituted benzylamine, K₂CO₃, KI (cat.) (for compounds **2–12**), dry acetonitrile, 30 min, 130 °C, MW.

Scheme 2. Synthesis of Compounds 42–43^a

^aReagents and conditions: (a) BH₃·SMe₂, THF, 0 °C to room temperature, 4 h; (b) 7-hydroxycoumarin, K₂CO₃, dry acetonitrile, 130 °C, 30 min, MW; (c) CBr₄, PPh₃, dry dichloromethane, 0 °C to room temperature, 4 h; (d) benzylamine or *N*-benzylmethylamine, K₂CO₃, dry acetonitrile, KI (cat.), 130 °C, 30 min, MW.

261 measured using Madin–Darby canine kidney (MDCK) cells,
262 retrovirally transfected with the human MDR1 cDNA
263 (MDCKII-MDR1). *P*_{app} and efflux ratio (ER) were calculated
264 and reported in Table 5.

Cytotoxicity of compound **37** was evaluated in human 265
neuroblastoma cell line SH-SY5Y through the 3-(4,5- 266
dimethylthiazol-2-yl)-2,5-diphenyl-tetrazolium bromide 267
(MTT) viability assay (Figure 8).⁷³ The same cell-based 268

Scheme 3. Synthesis of compounds 45^a

^aReagents and conditions: (a) (i) cinnamoyl chloride, dry dichloromethane, 4 h, reflux, (ii) AlCl₃, chlorobenzene, 8 h, reflux; (b) α,α' -dibromo-*p*-xylene, K₂CO₃, dry acetonitrile, 130 °C, 30 min, MW; (c) *N*-methylbenzylamine, K₂CO₃, dry acetonitrile, 130 °C, 30 min, MW.

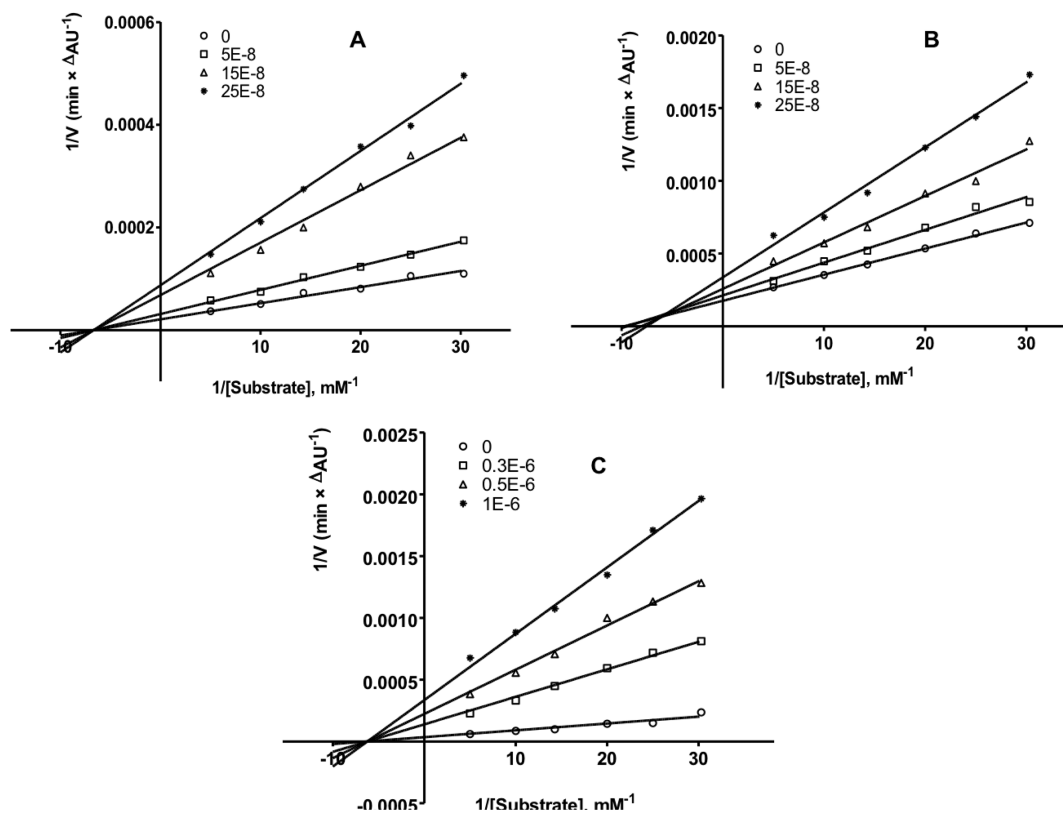


Figure 3. Lineweaver–Burk plots of inhibition kinetics of compounds 11 (A), 24 (B), and 37 (C). Reciprocals of enzyme activity (eeAChE) vs reciprocals of substrate (*S*-acetylthiocholine) concentration in the presence of different concentrations (0–250 nM) of inhibitor. Concentrations used for inhibitors are reported in inserts.

Table 5. Bidirectional Transport across MDCKII-MDR1 Cells of Compound 37

compd	P_{app} , AP-BL (cm/s)	P_{app} , BL-AP (cm/s)	ER ^a $P_{app, BL-AP}/P_{app, AP-BL}$
37	1.91×10^{-5}	3.38×10^{-5}	1.77
Diazepam	1.56×10^{-5}	1.23×10^{-5}	0.79
FD-4	1.13×10^{-6}	2.68×10^{-7}	0.23

^aEfflux ratio (ER) was calculated using the following equation: ER = P_{app} , BL-AP/ P_{app} , AP-BL, where P_{app} , BL-AP is the apparent permeability of basal-to-apical transport, and P_{app} , AP-BL is the apparent permeability of apical-to-basal transport. An efflux ratio greater than 2 indicates that a test compound is likely to be a substrate for P-gp transport.

269 method was used to for preliminarily investigate the
270 cytoprotective effects of compound 37 against cell death
271 induced by H₂O₂ (Figure 9).

272 ■ RESULTS AND DISCUSSION

273 For the sake of clarity, structure–activity and structure–
274 selectivity relationships (SAR and SSR, respectively) will be

discussed first separately for the different classes of compounds 275
reported in Tables 1–3, then a comparison will be made among 276
the inhibition data from rMAOs and eeAChE with the 277
corresponding data from hMAOs, hAChE and to a lesser 278
extent hBChE (Table 4). 279

**SARs and SSRs of *N*-Benzyl-*N*-alkoxy Coumarin 280
Derivatives (Table 1).** Compounds 2–12 were designed to 281
investigate the effects on inhibition potency and selectivity at 282
the target enzymes of the length of the polymethylene linker 283
and of the *N*-substitution at the NH-benzyl moiety with methyl 284
and ethyl groups. A few substituents were also introduced on 285
the benzyl ring of compound 6, bearing a pentamethylene 286
linker, to extend the knowledge of SARs and SSRs. 287

The inhibition data in Table 1 showed that, with a few 288
exceptions, the designed compounds display from low- to 289
submicromolar potencies against rMAO-B and eeAChE, 290
whereas potencies against rMAO-A and esBChE were slightly 291
lower. As the result, promising dual MAO-B and AChE 292
inhibitors were discovered with limited MAO-B over MAO-A 293
and AChE over BChE selectivity. 294

Interestingly, compounds 3, 5, 6, and 12, characterized by 295
linkers of different length, displayed submicromolar affinities at 296

Table 6. Analytical Data of Compounds 2–40, 42, 43, and 45

compd	melting point, °C (CC or cryst solvent) ^a	anal. calcd %			anal. found %		
		C	H	N	C	H	N
2 ^b	201–3 (CC)	68.12	6.76	3.61	68.10	6.86	3.73
3 ^b	183–5 (CC)	68.73	7.02	3.48	68.43	6.75	3.28
4	38–9 (CC)	75.59	7.45	3.83	75.78	7.55	3.61
5 ^b	238–40 (CC)	68.73	7.02	3.48	68.40	6.87	3.58
6	66–7 (CC)	75.96	7.70	3.69	75.58	7.45	3.80
7 ^b	247–9 (CC)	68.09	6.63	6.35	67.73	6.62	6.09
8 ^b	204–6 (CC)	64.00	6.49	3.11	63.94	6.35	2.98
9 ^b	201–3 (CC)	68.09	6.63	6.35	67.70	6.53	6.37
10 ^b	193–4 (CC)	69.83	7.50	3.26	69.55	7.37	3.31
11	54–5 (CC)	76.30	7.94	3.56	75.99	7.88	3.70
12 ^b	171–3 (CC)	70.33	7.72	3.15	70.51	8.03	3.48
13	181–2 (EtOH)	73.77	6.19	4.53	73.42	6.36	4.24
14 ^b	225–7 (EtOH)	67.46	6.47	3.75	67.27	6.50	3.79
15	156–7 (CC)	71.67	6.01	3.63	71.29	5.78	3.31
16 ^b	132–4 (EtOH)	69.87	5.19	6.27	69.51	5.54	6.03
17 ^b	121–3 (EtOH)	69.10	5.80	3.10	68.81	5.64	3.31
18 ^b	131–3 (EtOH)	65.80	5.08	3.07	65.55	5.29	3.31
19	108–9 (EtOH/Et ₂ O)	73.77	6.19	4.53	73.88	6.41	4.35
20	167–8 (EtOH/Et ₂ O)	74.75	6.87	4.15	74.93	6.47	4.01
21	106–7 (EtOH)	71.67	6.01	3.63	71.44	5.89	3.55
22 ^b	>250 (CC)	71.63	6.01	3.21	71.31	5.95	3.26
23 ^b	>250 (CC)	71.63	6.01	3.21	71.37	6.06	3.34
24 ^b	226–8 (CC)	72.07	6.27	3.11	71.77	6.23	3.14
25 ^b	129–31 dec. (EtOH)	69.87	5.19	6.27	69.64	5.33	6.40
26 ^b	128–30 (EtOH)	69.10	5.80	3.10	69.34	5.51	3.23
27 ^b	124–6 (CC)	65.80	5.08	3.07	65.97	5.35	3.19
28 ^b	>250 (CC)	66.39	5.36	2.98	66.04	5.29	2.80
29 ^b	247–50 dec (CC)	66.39	5.36	2.98	65.99	5.39	2.80
30 ^b	236–8 (CC)	66.95	5.62	2.89	67.31	5.80	3.22
31 ^b	147–9 (CC)	69.87	5.19	6.27	70.12	5.29	6.37
32 ^b	242–4 (CC)	70.35	5.47	6.08	69.99	5.49	6.10
33 ^b	224–6 (CC)	70.35	5.47	6.08	70.72	5.59	6.12
34 ^b	225–7 (CC)	70.80	5.73	5.90	70.55	5.97	5.76
35 ^b	155–7 dec. (CC)	69.87	5.19	6.27	69.46	5.55	5.92
36 ^b	183–5 dec. (CC)	68.72	4.70	8.90	68.88	4.79	8.59
37 ^b	235–6 dec. (CC)	69.10	5.80	3.10	69.15	5.71	3.43
38	109 dec, 130–2 (EtOH)	74.80	5.77	3.49	74.44	5.69	3.47
39 ^b	231–36 (CC)	64.20	5.18	2.88	63.80	5.13	2.89
40 ^b	150–2 (CC)	67.99	5.28	5.87	67.61	5.29	5.56
42 ^b	207–9 (CC)	71.63	6.01	3.21	71.81	5.91	3.01
43 ^b	>250 (CC)	71.17	5.73	3.32	71.27	5.47	3.37
45 ^b	154–5 ^c (CC)	71.33	5.99	6.65	71.61	6.04	6.32

^aCC: column chromatography (see Supporting Information for details). ^bHydrochloride salt. ^cFree base.

297 both rMAO-B and eeAChE with a limited selectivity over
 298 rMAO-A and esBChE, respectively. The gradual elongation of
 299 the linker in the *N*-Me derivative **2**, affording compounds **4**, **6**,
 300 and **11**, provided a consistent increase of potency toward
 301 eeAChE (from 1.3 μ M of **2** to 0.095 μ M of **11**) and esBChE
 302 (from 7.8 μ M of **2** to 0.67 μ M of **11**), whereas an opposite
 303 effect was observed with rMAO-B (from 0.33 μ M of **2** to 1.7
 304 μ M of **11**). Therefore, in this series of compounds, the goal of
 305 optimizing both MAO-B and AChE activities could not be
 306 achieved by varying the length of the linker. However, moving
 307 from the *N*-methyl derivative **11** to the *N*-ethyl homologue **12**
 308 good activities at the three target enzymes, rMAO-B, eeAChE,
 309 and esBChE, were obtained but along with a very low MAO-B
 310 over MAO-A selectivity (SI = 3; SI is the selectivity index
 311 calculated as the ratio IC₅₀ MAO-A/IC₅₀ MAO-B). Compound

11 was endowed with the highest eeAChE inhibitory potency 312
 within the whole examined series (IC₅₀ = 0.095 μ M) and, 313
 surprisingly, the highest rMAO-A inhibitory potency (IC₅₀ = 314
 0.51 μ M) leading to a reversal of rMAO selectivity (SI = 0.3). 315
 Kinetics of eeAChE inhibition resulted in a mixed-type 316
 mechanism, as expected from putative dual binding site 317
 inhibitors (Figure 3A), with *K_i* equal to 0.080 ± 0.002 μ M. 318

Notably, compounds with the longest linker **11** and **12** 319
 displayed the highest inhibitory potency on rMAO-A (IC₅₀ = 320
 0.51 and 2.1 μ M, respectively) and ChEs (IC₅₀ = 0.095 and 321
 0.32 μ M, respectively, at AChE, and 0.67 and 0.49 μ M, 322
 respectively, at BChE). No clear relationship emerged from the 323
 comparison of inhibition potency of *N*-methyl and *N*-ethyl 324
 derivatives. 325

The introduction in compound **6** of a cyano group in position *meta* and *para* (**7** and **9**, respectively) and of a chlorine at position *meta* (compound **8**) did diminish the inhibitory potency toward all the tested enzymes except for compound **8** at both ChEs.

SARs and SSRs of *meta*- and *para*-*N,N*-Dialkylamino-methyl-7-benzoyloxycoumarin Derivatives (Table 2).

Compounds **13**–**40** were designed to investigate the effects on inhibition potency and selectivity at the three target enzymes of the *N,N*-dialkylaminomethyl substituents at the *meta* and *para* positions of the 7-benzoyloxy moiety and of substituents at position 3 and 4 of the coumarin ring, having in mind our previous findings,^{68,69} which highlighted the steric requirements for this region in binding MAO-B enzymatic cleft. A number of substituents were also introduced on the *N*-benzyl ring in R_4 to extend the study of SARs and SSRs.

It is worth underlining that all the examined compounds shared a *meta*- or *para*-xylyl linker joining the oxygen at position 7 of coumarin with the basic *N,N*-dialkylamino substituents. Both xylyl linkers have a lower conformational flexibility compared to the polymethylene linkers of compounds **2**–**12**, and this might result in a higher (iso)enzyme selectivity. Indeed, this was the case for rMAOs, as most compounds achieved micromolar to submicromolar rMAO-B inhibitory potency whereas an inhibition lower than 20% at 10 μM was generally displayed at rMAO-A. The same effect on selectivity was not observed for the ChEs even though most compounds appeared slightly more AChE-selective. Inhibition potency on eeAChE reached the submicromolar level in 11 cases, the most potent inhibitor being compound **24** ($\text{IC}_{50} = 0.10 \mu\text{M}$), while on esBChE only six compounds exhibited a submicromolar activity, with compound **19** showing the highest potency ($\text{IC}_{50} = 0.24 \mu\text{M}$).

As the *N,N*-dimethylaminomethyl derivative **13**, the lead compound of the *meta*-xylyl series, showed very low inhibitory effect on rMAO-A and eeAChE ($\text{IC}_{50} = 10 \mu\text{M}$ and 38% inhibition at 10 μM , respectively) and moderate activity on rMAO-B and esBChE ($\text{IC}_{50} = 3.2$ and $5.3 \mu\text{M}$, respectively), its *N,N*-diethylamino **14** and *N*-methyl-*N*-benzylamino **15** congeners were synthesized. Improved potencies were definitely gained with compound **15** that showed an interesting profile of inhibition with low micromolar potencies rMAO-B, eeAChE, and esBChE ($\text{IC}_{50} = 2.0$, 2.3 , and $1.0 \mu\text{M}$, respectively) and very weak activity at rMAO-A (8% inhibition at 10 μM). The introduction of cyano, methoxy, and chloro substituents at the *meta* position of the phenyl ring of the *N*-benzylamino moiety, leading to compounds **16**, **17** and **18**, respectively, resulted in lower inhibitory potencies on rMAO-B and eeAChE, whereas a 3-fold increased inhibition was observed for the chloro derivative **18** on esBChE ($\text{IC}_{50} = 0.31$ vs $1.0 \mu\text{M}$).

The *para*-*N,N*-dimethylamino- and *N,N*-diethylamino-methyl derivatives **19** and **20** displayed lower activity against rMAO-A, similar activity against rMAO-B, and higher activity against esBChE when compared to the corresponding *meta*-substituted isomers **13** and **14**. Better results were obtained with the *para*-*N*-methyl, *N*-benzylaminomethyl derivative **21** that achieved submicromolar potency toward rMAO-B and eeAChE ($\text{IC}_{50} = 0.85$ and $0.75 \mu\text{M}$, respectively) and a significantly lower activity against rMAO-A and esBChE (7% at 10 μM and $\text{IC}_{50} = 11 \mu\text{M}$, respectively).

Methyl substituents were introduced at the positions 3 and 4 of the coumarin ring to give the monomethyl derivatives **22** and **23** and the dimethyl derivative **24**. Compared to the lead

compound **21**, the rMAO-B activity decreased while a significant increase of the inhibitory potency on eeAChE ($\text{IC}_{50} = 0.26$, 0.18 , and $0.10 \mu\text{M}$) and esBChE ($\text{IC}_{50} = 1.1$, 1.0 , and $0.69 \mu\text{M}$) was observed for compounds **22**, **23**, and **24**, respectively. It is worth noting that these very simple structural changes led to the most potent eeAChE inhibitors of the whole series of compounds and, even more interestingly, for compound **24** an impressive combination of high inhibitory activities toward rMAO-B, eeAChE, and esBChE and high rMAO-B-selectivity was revealed ($\text{IC}_{50} = 1.2$, 0.10 , and $0.69 \mu\text{M}$ at rMAO-B, eeAChE, and esBChE, respectively, and 0% inhibition at 10 μM at rMAO-A). As for open chain derivative **11**, also compound **24** displayed mixed-mode kinetics for eeAChE inhibition, with K_i equal to $0.22 \pm 0.03 \mu\text{M}$ (Figure 3B).

As done for lead compound **15**, the isomeric compound **21** was modified by introducing cyano, methoxy, and chloro substituents at position *meta*, and the cyano group at position *para* as well, in the aromatic ring of the *N*-benzylamino moiety. *Meta*-substituted derivatives **25**–**27** proved to be less potent inhibitors than the lead compound **21** on rMAO-B. *Meta*-chloro derivative **27** maintained, however, an attractive inhibition profile (12% inhibition at 10 μM at rMAO-A; $\text{IC}_{50} = 2.7$, 0.59 , and $1.2 \mu\text{M}$, at rMAO-B, eeAChE, and esBChE, respectively). Therefore, compound **27** was slightly modified by introducing methyl substituents at the positions 3 and 4 to afford the monomethyl derivatives **28** and **29** and the dimethyl derivative **30**. Compared to **27**, rMAO-B, rMAO-A, and esBChE activities considerably decreased, while the potency toward AChE was maintained, or even improved, in particular for the 4-methyl derivative **29** ($\text{IC}_{50} = 0.12$ vs $0.59 \mu\text{M}$). Compared to **21**, 4-cyanobenzylamino derivative **31** displayed lower activities toward rMAO-A, eeAChE, and esBChE and a 3-fold increase of rMAO-B activity. The introduction in compound **31** of methyl substituents at the positions 3 and 4, to give the monomethyl derivatives **32** and **33** and the dimethyl derivative **34**, generally diminished the activity on almost all enzymatic targets.

The final structural modifications of lead compound **21** were aimed at reducing molecular lipophilicity while maintaining good inhibitory activities on the target enzymes. One approach aimed at the modulation of the pK_b of the basic head, through the elongation of an arm of the linker that allowed a higher distance between the two electron withdrawing phenyl rings from the basic nitrogen, resulting in lower pK_b and $\log D$. This structural modification increased the distance between the two key binding moieties of **21**, that is, the coumarin ring and the *N*-benzyl group, giving rise to the more flexible *N*-benzyl, *N*-phenethyl analogue **42** (Table 3). In addition, *N*-demethylated derivative **43** was synthesized to test the effect of having a more hydrophilic basic moiety endowed with HB-donor ability. Compared to compound **21**, the homologue **42** showed a similar activity toward eeAChE ($\text{IC}_{50} = 0.85$ vs $0.75 \mu\text{M}$) and rMAO-A (12% vs 7%), a much higher activity at esBChE ($\text{IC}_{50} = 0.52$ vs $11 \mu\text{M}$), and a decreased activity at rMAO-B ($\text{IC}_{50} = 4.1$ vs $0.85 \mu\text{M}$). To our surprise, the *N*-demethylated congener **43** reversed MAO selectivity, being the activity on rMAO-A higher than that on rMAO-B ($\text{IC}_{50} = 1.7 \mu\text{M}$ and 45% inhibition at 10 μM , respectively). The inhibition potency on eeAChE worsened ($\text{IC}_{50} = 4.7$ vs $0.85 \mu\text{M}$), while conversely the potency against esBChE remained nearly unchanged ($\text{IC}_{50} = 0.64$ vs $0.52 \mu\text{M}$). An additional less lipophilic analogue of **21**, namely **45** in Table 3, was prepared through bioisosteric

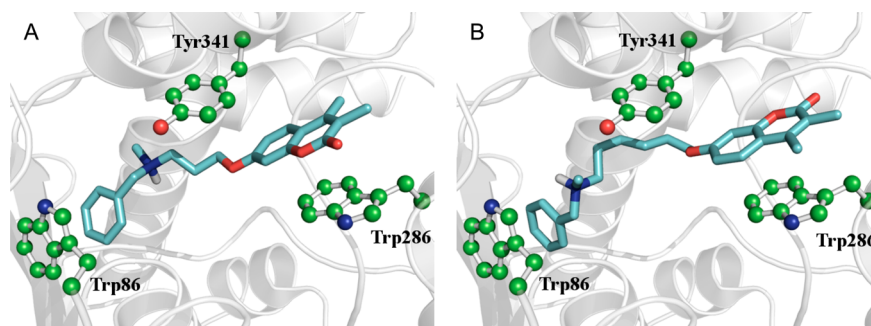


Figure 4. Docking poses of inhibitor **2** (A) and **11** (B) into human AChE binding site (PDB code: 4EY7). Inhibitors are represented in sticks, while relevant amino acid residues are in ball-and-sticks, colored according to the atom code (C atoms in cyan and green for inhibitors and amino acid residues, respectively). Docking scores are equal to -98.2 and -106.2 kJ/mol for inhibitor **2** and **11**, respectively.

452 replacement of the 2*H*-chromen-2-one with the 2-quinolone as
 453 successfully done in the past for a dual binding site AChE
 454 inhibitor.²¹ Actually, the activity toward both cholinesterases
 455 improved ($IC_{50} = 0.49$ vs 0.75 μ M and 1.7 vs 11 μ M at eeAChE
 456 and esBChE, respectively) and the low activity on rMAO-A was
 457 maintained but, unexpectedly, the activity on rMAO-B
 458 dramatically decreased (29% inhibition at 10 μ M vs $IC_{50} =$
 459 0.85 μ M).

460 As the homologation of the basic head and the isosteric
 461 replacement yielded unsatisfying results, compound **21** was
 462 modified by introducing polar groups on the coumarin core.
 463 The insertion of a polar cyano group on the coumarin ring at
 464 position 3 (comp. **35**) was highly detrimental for rMAO-B
 465 activity (41% at 10 μ M vs $IC_{50} = 0.85$ μ M), while a 3- and 2-
 466 fold potency increase was observed against eeAChE ($IC_{50} =$
 467 0.20 vs 0.75 μ M) and esBChE ($IC_{50} = 5.5$ vs 11 μ M),
 468 respectively. Better results on rMAO-B but much worse toward
 469 both ChEs came from the introduction of a second polar
 470 substituent, a *para*-cyano group on the *N*-benzyl ring (comp.
 471 **36**).

472 Guided by docking simulations and a 3D-QSAR model
 473 recently developed from a large series of 4,7-disubstituted
 474 coumarins,⁶⁹ a different, more polar substituent, that is the
 475 hydroxymethyl group, was introduced at position 4 of the
 476 coumarin core. Very satisfactorily, inhibitor **37** showed good
 477 inhibitory activities with the three target enzymes ($IC_{50} = 0.41$,
 478 0.42 , and 1.1 μ M at rMAO-B, eeAChE, and esBChE,
 479 respectively) and no activity on rMAO-A (0% inhibition at
 480 10 μ M). As for compounds **11** and **24**, also **37** showed a mixed-
 481 type inhibition mode (Figure 3C), with a K_i equal to $0.10 \pm$
 482 0.01 μ M. The *N*-demethylated derivative of **37**, that is
 483 compound **38**, was also prepared and tested. Its inhibitory
 484 potencies and selectivity profile ($IC_{50} = 0.53$, 0.44 , and 0.57 μ M
 485 at rMAO-B, eeAChE, and esBChE, respectively, and 19%
 486 inhibition at rMAO-A at 10 μ M) were very good and compared
 487 well with those of the *N*-methyl analogue.

488 As previous SAR/3D-QSAR⁴⁵ and current docking studies
 489 (data not shown) suggested favorable interactions of a halogen
 490 atom at the *meta* position of a benzyl ring at AChE and MAO-B
 491 binding sites, the *meta*-chloro derivative **39** was synthesized and
 492 tested. Its excellent inhibitory activities on the three target
 493 enzymes ($IC_{50} = 0.24$, 0.25 , and 0.63 μ M for rMAO-B,
 494 eeAChE, and esBChE, respectively, and 0% inhibition toward
 495 rMAO-A at 10 μ M) proved the goodness of our molecular
 496 design. Indeed, compound **39** attained the pursued combina-
 497 tion of strong and well-balanced inhibitory potencies and an
 498 excellent rMAO-B over rMAO-A selectivity.

The introduction of a *para*-cyano substituent in the *N*-benzyl
 499 ring of **37** led to **40**, which showed an exquisite rMAO-B
 500 activity and selectivity (rMAO-B, $IC_{50} = 0.035$ μ M; rMAO-A,
 501 0% inhibition at 10 μ M) but also a dramatic drop of activity at
 502 eeAChE ($IC_{50} = 6.3$ μ M) and esBChE (23% inhibition at 10
 503 μ M), indeed resulting as the most potent MAO-B inhibitor of
 504 the whole set of compounds herein investigated. 505

Inhibitory Activities on Human Enzymes. The good
 506 biological profiles of many inhibitors toward MAO and ChE
 507 enzymes, prompted us to extend our inhibition assays to the
 508 corresponding human enzymes. On the basis of our previous
 509 studies,⁷² significant changes of inhibitory activities were
 510 expected for hMAOs (generally an improvement, especially at
 511 hMAO-B), whereas more limited differences were awaited for
 512 hAChE inhibition. However, to gain further support to these
 513 general predictions and select compounds with high activity on
 514 hMAO-B and hAChE, a prospective docking study was
 515 performed on the series of inhibitors listed in Table 4. 516
 517 Inhibition activities on human enzymes were not assessed for
 518 compounds exhibiting low potency against the corresponding
 519 rMAO and eeAChE enzymes. 519

Prospective docking simulations were carried out using
 520 GOLD Suite v5.2⁷⁴ on the X-ray crystal structures of AChE and
 521 MAO-B available from the PDB. For AChE studies, the X-ray
 522 crystal structures of *Torpedo californica* AChE (TcAChE) (PDB
 523 entry: 1EVE) and human recombinant AChE (hAChE) (PDB
 524 entry: 4EY7), both complexed with donepezil, were used. The
 525 careful inspection of the two crystal structures revealed that
 526 PAS and CAS binding sites of AChE are at about 18 Å distance
 527 (measured between the $C\alpha$ carbon atoms of Trp86 and Trp286
 528 of hAChE). Distances between the two putative binding
 529 moieties close to such a value might ensure efficient
 530 interactions at both PAS and CAS. On this basis, we conceived
 531 predictive docking studies aimed at forecasting the optimal
 532 length of the polymethylene spacer joining the pharmacophore
 533 features, ensuring strong AChE binding. In this respect, the in
 534 silico studies were focused on two compounds (**2** and **11** of
 535 Table 1), bridging the protonatable basic tail and the coumarin
 536 head with a short (trimethylene) or long (hexamethylene)
 537 linear linker, respectively. Interestingly, docking simulations
 538 returned similar poses for the two compounds, which were
 539 both able to engage steady π - π stacking interactions with the
 540 aromatic residues of Trp86 and Trp286. The compound
 541 bearing the longer linear linker showed a higher score (-106.2
 542 kJ/mol for hAChE and -96.3 kJ/mol for TcAChE) compared
 543 to that bearing the shorter linker (score: -98.2 kJ/mol for
 544 hAChE and -88.6 kJ/mol for TcAChE). For clarity, a zoomed
 545 44

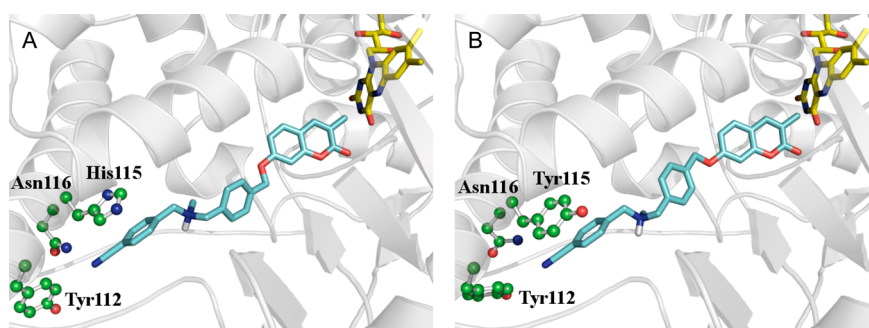


Figure 5. Docking poses of inhibitor **32** into human (PDB code: 2V60) (A) and rat MAO-B (homology model) (B) binding sites. Inhibitors and FAD cofactor are represented in sticks, while relevant amino acid residues are in ball-and-sticks, colored according to the atom code (C atoms in cyan, yellow, and green for inhibitors, cofactor, and amino acid residues, respectively). Docking scores are equal to -88.21 and -80.22 kJ/mol for inhibitor **32** into human and rat isoforms, respectively.

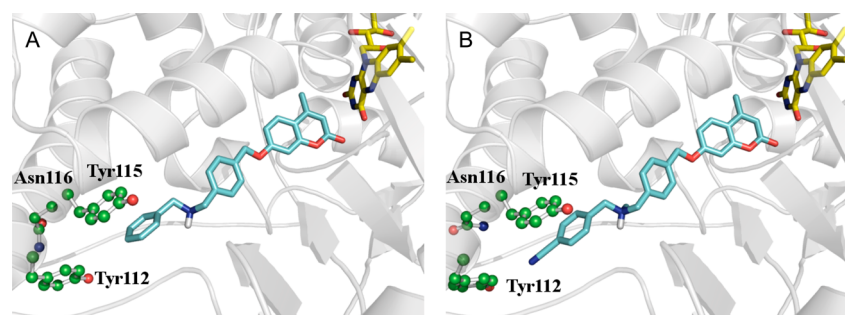


Figure 6. Docking poses of inhibitor **23** (A) and **33** (B) into rat MAO-B binding site (homology model). Inhibitors and FAD cofactor are represented in sticks, while relevant amino acid residues in ball-and-sticks, colored according to the atom code (C atoms in cyan, yellow, and green for inhibitors, cofactor, and amino acid residues, respectively).

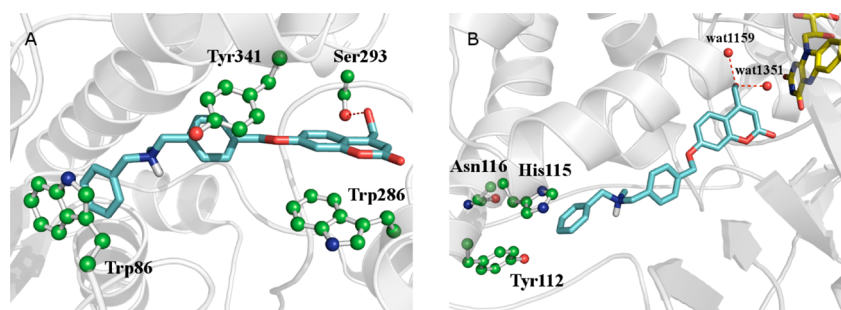


Figure 7. Docking poses of inhibitor **37** into (A) hAChE (PDB code: 4EY7) and (B) hMAO-B (PDB code: 2V60) binding sites. Inhibitors are represented in sticks, while relevant amino acid residues in ball-and-sticks, colored according to the atom code (C atoms in cyan and green for inhibitors and amino acid residues, respectively). Structural water molecules (that are HOH1159 and HOH1351 according to the numbering of 2V60) are represented as red balls. Hydrogen bonds are represented as red dashed lines. Docking scores are equal to -109.38 and -95.95 kJ/mol for inhibitor **37** into hAChE and hMAO-B, respectively.

in view of top-scored solutions is shown in Figure 4. Compounds **2** and **11** actually proved effective in inhibiting AChE, in good agreement with the docking scores.

For MAO-B studies, the X-ray crystal structure of hMAO-B (PDB entry: 2V60) and a homology model for the rMAO-B were used. We performed a number of exploratory docking runs to assess whether the decoration of the well-known 7-benzyloxycoumarin with a protonatable amino tail (mimicking the basic head of donepezil) could be suitable in biasing also MAO-B. To this end, we docked three probe compounds (**23**, **32**, and **33** in Table 2) into the binding site of MAO-B and observed that the ad hoc incorporated benzylamine fragment was located in a peripheral region surrounded by Tyr112, His115 (mutated to Tyr115 in rMAO-B), and Asn116. As shown in Figure 5, the residue at position 115 is critical in

establishing π - π stacking interactions with the terminal benzyl ring of **32**, although the scores at hMAO-B were consistently higher than those at rMAO-B. These interspecies differences were even more pronounced in enzyme inhibition potency of **32**, showing two log units higher activity at hMAO-B compared to rMAO-B ($IC_{50} = 0.017$ vs $1.7 \mu\text{M}$). We hypothesized that such scoring and biological differences in hMAO-B and rMAO-B can rely on a likely greater strength of the π - π stacking interactions engaged by the imidazole ring of His115 compared to that of the phenyl ring of Tyr115.⁷⁵

The potential benefit of introducing a cyano group at the *para* position of the benzylamine was also challenged by docking compounds **23** and **33**. Actually, we did not observe any appreciable difference in the scores; however, the presence of the cyano group increased the rMAO-B inhibition

576 approximately 10-fold (**23**, $IC_{50} = 4.1 \mu M$ vs **33**, $IC_{50} = 0.41$
577 μM). We tentatively explained this experimental result by
578 visually inspecting the docking poses of **23** and **33**. As shown in
579 Figure 6, the cyano group could form HBs (even water-
580 mediated) with Asn116 or Tyr112.

581 For the sake of completeness, additional modeling studies
582 were conducted on **37**, one of the most potent multitarget
583 inhibitors of the series. **37** was first docked into both hAChE
584 and TcAChE to assess the binding interactions resulting from
585 the substitution of an aliphatic linker with an aromatic one and
586 of the 4-H atom with a more polar 4-hydroxymethyl group.
587 Beyond hydrophobic interactions already described for
588 inhibitors **2** and **11** bearing an aliphatic linker, inhibitor **37**
589 was engaged in a $\pi-\pi$ interaction involving the *para*-xylyl linker
590 and the aromatic side chain of Tyr341 (hAChE numbering
591 referred to PDB entry 4EY7).¹⁷ In addition, a HB occurred
592 between the 4-hydroxymethyl group and Ser293 of hAChE as
593 shown in Figure 7A. The higher score of **37** toward hAChE
594 (-109.38 kJ/mol) compared to **2** and **11** may be therefore
595 ascribed to both $\pi-\pi$ and HB interactions (Figure 7A).

596 As reported in previous studies,^{68,69} the introduction of polar
597 groups at position 4 of the coumarin scaffold improved
598 physicochemically relevant properties (e.g., aqueous solubility
599 and lipophilicity) while maintaining good MAO-B inhibitory
600 potency and selectivity. Thus, inhibitor **37** was docked also on
601 hMAO-B, resulting in a binding pose similar to that of **23**, **32**,
602 and **33** but with a higher score (-95.95 kJ/mol). Most likely
603 the high hMAO-B inhibitory potency arose from the formation
604 of multiple HBs between the hydroxyl group and structural
605 water molecules^{45,49,68} as illustrated in Figure 7B.

606 Inhibition data in Table 4 fulfilled our expectations and
607 docking calculations. As far as the inhibitory activities on
608 hMAO-B are concerned, a consistent increase of activity, from
609 2.5-fold for compound **2** up to 121-fold for **34**, was recorded,
610 whereas the activities on hMAO-A remained low or were
611 slightly incremented, from 2.7-fold for compound **11** to 18-fold
612 for compound **12**. As the result, the hMAO-B over hMAO-A
613 selectivity strongly raised. Actually, the SIs measured for
614 compounds **37**, **39**, and **40** were 2210, 842, and 910,
615 respectively. Because many other inhibitors activities on
616 hMAO-A remained very low, the IC_{50} values were not
617 measured and the hMAO selectivity could not be exactly
618 assessed. Nevertheless, taking into account the low percentage
619 of inhibition of hMAO-A at $10 \mu M$ concentration, high hMAO-
620 B over hMAO-A selectivity can be confidently foreseen also for
621 inhibitors **21**, **31**, and **32**.

622 It is worth noting that all the coumarin derivatives listed in
623 Table 4 attained submicromolar inhibitory on hMAO-B.
624 Coumarin derivatives **37** and **40**, bearing the 4-CH₂OH
625 group, were the most potent inhibitors within the whole
626 molecular series examined, with IC_{50} values in the low
627 nanomolar range (10 and 5.7 nM, respectively). Interestingly,
628 some similarities and striking differences emerged by
629 comparing inhibitory activities at rat and human MAO
630 enzymes. For instance, 4-CH₂OH-bearing coumarin derivatives
631 **37**, **39**, and **40** resulted in the most active MAO-B inhibitors at
632 both the human and rat enzymes, with compound **40** showing
633 the highest activities ($IC_{50} = 0.0057$ and $0.035 \mu M$,
634 respectively). It is noteworthy that the inverted selectivity
635 observed on rMAOs for compound **11**, bearing the longest
636 polymethylene linker, was maintained also on hMAOs.

637 As anticipated in the Introduction, the selective inhibition of
638 either AChE or BChE was not a primary aim of our work.

Nonetheless, a number of representative compounds, that is **5**, **39**
11, **21**, **24**, **37**, and **39**, were tested also on hBChE (Table 4).
Despite an 89.4% of amino acid sequence identity, the human
and equine enzymes displayed significant differences in the
catalytic site and even more in the peripheral sequence.
Notably, Gly277, Pro285, and Phe398 in human mutated to
Asp, Leu, and Ile, respectively, in equine. The amino acid
numbering refers to hBChE as reported in PDB. Therefore,
different inhibition potencies at the two enzymes may be
expected and this was indeed observed for compounds **24**, **39**,
21, and **37** (46% and 14% at $10 \mu M$ and $IC_{50} = 0.89$ and 9.3
 μM versus $IC_{50} = 0.69$, 0.63 , 11 , and $1.1 \mu M$, respectively). In
contrast, compounds **5** and **11** displayed submicromolar
inhibition potencies on hBChE close to the ones observed on
esBChE.

Appealing inhibition profiles resulted for compounds **5**, **37**,
and **39**. The first displayed submicromolar potencies at all the
four tested human enzymes, along with a significant, but
limited, selectivity for hMAO-B (SI = 13.5) and no selectivity
for either one of the two ChEs. The latter two showed high
hMAO-B inhibitory potencies and selectivities ($IC_{50} = 10$ and
 24 nM, and SI = 1580 and 542, respectively) and also a good
hAChE inhibitory potency and selectivity ($IC_{50} = 0.12$ and 0.33
 μM , and SI = 77.5 and $\gg 30$, respectively).

Taking into account inhibition potencies, selectivity data, and
physicochemical parameters, inhibitor **37** was selected for a
preliminary evaluation of its ability to cross blood-brain barrier
(BBB) and its cytotoxicity and cytoprotective properties.

■ BBB PERMEABILITY AND TOXICITY PROFILING OF COMPOUND 37

MDCK-MDR1 cell lines are known to express P-glycoprotein
(P-gp), which plays an important role in the efflux transport of
drugs from brain to blood. Thus, we were particularly interested
to see if compound **37** was able to permeate by passive
diffusion the BBB and to interact with P-gp as well. To this
purpose, transport studies were performed on MDCKII-MDR1
cells which are characterized by high P-gp expression and
represent a well-established in vitro model mimicking the
BBB.^{76,77} Transport studies were conducted in both apical-to-
basal (AP-BL) and basal-to-apical (BL-AP) directions, and the
results were reported in Table 5. Fluorescein isothiocyanate-
dextran (FD4) and diazepam were used as paracellular and
transcellular markers, respectively, of cell monolayers' integrity
and as internal controls to verify tight junction integrity during
the assay; the results for controls were within the expected
values. Both apparent permeabilities (AP-BL, $1.91 \times 10^{-5} \text{ cm}^2$
 s^{-1} ; BL-AP, $3.38 \times 10^{-5} \text{ cm}^2 \text{ s}^{-1}$) were comparable with those of
diazepam, thus supporting a good BBB penetration. The efflux
ratio (ER) equal to 1.77 detected for compound **37** disclosed
no significant differences in P_{app} values between AP-to-BL and
BL-to-AP direction. Because a value of ER greater than 2
indicates that a test compound is likely to be a substrate for P-
gp transport, the measured value suggested that compound
should be able to permeate the monolayer without significant
interactions with such efflux system.

The effects of compound **37** on the viability of human
neuroblastoma cell line SH-SY5Y were studied, using donepezil
as reference compound. As shown in Figure 8, compound **37**,
like donepezil, was not cytotoxic at the tested concentrations
ranging from 0.1 to $50 \mu M$ after 24, 48, and 72 h of incubation.
The neuroprotective capacity of **37** against oxidative stress was
also evaluated using the same cell line and hydrogen peroxide

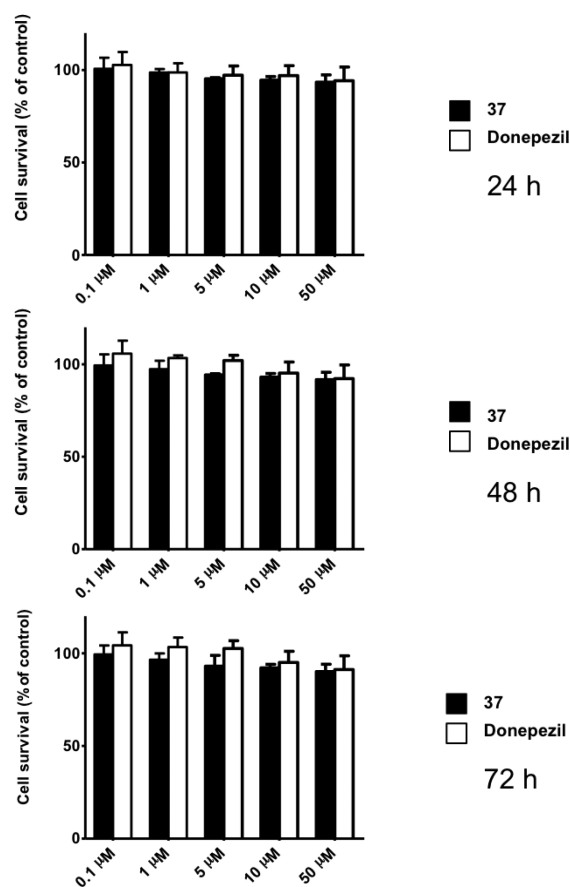


Figure 8. Viability of human neuroblastoma SH-SY5Y cells exposed to compound 37 at different concentrations and incubation times. SH-SY5Y cells were incubated with increasing concentrations (range 0.1–50 μM) of the test compounds for 24, 48, and 72 h. Untreated cells were used as control. Results are expressed as percentage of viable cells observed after treatment with compounds 37 and donepezil vs untreated control cells (100%) and shown as mean \pm SD ($n = 3$).

701 (H_2O_2) for the generation of exogenous free radicals. Cells
 702 were incubated with 37 at two nontoxic concentrations (1 and
 703 10 μM) for 24 h, then, H_2O_2 (60 μM) was added and the cells
 704 maintained for further 24 h. Cell death was determined using
 705 the MTT assay. As shown in Figure 9, compound 37 at 10 μM
 706 concentration prevented the H_2O_2 -induced cell death (ca. 25%)
 707 with a statistically significant effect ($P < 0.01$).

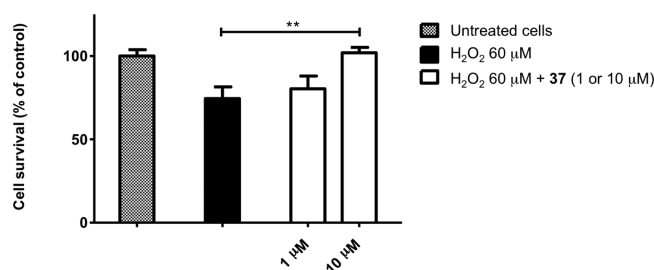


Figure 9. Percentage of cell survival in the human neuroblastoma cell line SH-SY5Y of compounds 37 in the following conditions: untreated cells (gray column), in the presence of H_2O_2 (60 μM) alone (black column), in the presence of both H_2O_2 (60 μM), and compound 37 (1 and 10 μM , white columns). Data represent means \pm SD ($n = 3$); statistical significance was estimated using one-way ANOVA and Bonferroni post hoc test (** $P < 0.01$).

CONCLUSIONS

708

The most salient features emerging from the SARs and SSRs of the two classes of compounds examined in this paper can be summarized as follows. Highly flexible inhibitors of the *N*-benzyl, *N*-alkoxy coumarin series in Table 1 showed good inhibitory activities at the target enzymes when bearing a penta- or hexamethylene linkers but low selectivity (see compounds 6, 11, and 12 in Table 1). The inhibitors bearing a more rigid xylyl linker (Table 2) displayed good inhibitory potencies and high rMAO-B over rMAO-A selectivity ratios. Compound 21, a more rigid analogue of 6, exhibited good activities and selectivity toward rMAO-B and eeAChE. *Meta*-chlorobenzyl analogues (i.e., 27, 35, and 39) showed an improved inhibition at eeAChE and esBChE but a worse inhibition at rMAO-B, whereas in contrast the *para*-cyanobenzyl analogues 31, 33, and 36 showed better potencies toward rMAO-B and decreased potencies toward eeAChE. The more polar and hydrophilic 4-hydroxymethyl derivatives 37–39 displayed the most interesting activity profiles with low submicromolar activity at the three target enzymes rMAO-B, eeAChE, and esBChE and low or no activity at rMAO-A.

More interesting results came from the assays of selected inhibitors on human MAOs and AChE. In comparison with nonhuman enzymes, a significant increase of inhibitory activities was observed for hMAOs, more pronounced on hMAO-B, with a consequent increase of the selectivity index. More limited variations, generally a decrease of inhibitory potency, were instead observed with hAChE and hBChE. The most interesting inhibitors, e.g., 5, 12, 21, and 37–39, showed excellent activity profiles with low nanomolar inhibitory potency on hMAO-B, high MAO-B over MAO-A selectivity, and submicromolar potency on hAChE. Kinetic inhibition data and docking studies on selected compounds suggested a mixed-type mechanism of inhibition and binding interactions at both the CAS and PAS of AChE. Therefore, our compounds do behave as dual binding site inhibitors and have the potential to block another pathological mechanism of AD, that is, the AChE-promoted A-beta aggregation taking place at the PAS.^{78,79}

Ultimately, our hybridization strategy proved successful in designing and optimizing novel coumarin-containing compounds targeting MAO-B and ChEs, two key enzymes involved in AD, PD, and other neurodegenerative diseases, with well-balanced inhibition potencies. Activity, selectivity, and physicochemical properties were improved compared to other ligands targeting the same enzymes described so far.^{53–57} Moreover, toxicity, neuroprotection, and transport data, as preliminarily assessed using cell-based models, suggested that the 4-hydroxymethyl coumarin derivative 37, which resulted the most promising inhibitor, is devoid of significant neurotoxicity, shows moderate neuroprotective effects against H_2O_2 -induced cell death, as well as a good BBB permeability profile with limited P-gp affinity.

In conclusion, some of the multipotent inhibitors reported herein, and compound 37 in particular, may be considered promising leads for further preclinical studies in cognitive and neurodegenerative disease models.

EXPERIMENTAL SECTION

765

Chemistry. Starting materials, reagents, and analytical grade solvents were purchased from Sigma-Aldrich Europe. All reactions were routinely checked by TLC using Merck Kieselgel 60 F254 aluminum plates and visualized by UV light. Microwave reactions were

770 performed in a Milestone MicroSynth apparatus, setting temperature
771 and hold times, fixing maximum irradiation power to 500 W and
772 heating ramp times to 2 min. The purity of all the intermediates was
773 checked by ^1H NMR and ESI-MS. ESI-MS analyses were performed
774 on an Agilent 1100 LC-MSD trap system VL. Flash chromatographic
775 separations were performed on a Biotage SP1 purification system using
776 flash cartridges prepacked with KP-Sil 32–63 μm , 60 \AA silica.
777 Elemental analyses were performed on a EuroEA 3000 analyzer only
778 on the final compounds and are reported in Supporting Information.
779 The measured values for C, H, and N agreed to within $\pm 0.40\%$ of the
780 theoretical values. Melting points (MP) were taken on a Gallenkamp
781 MFB 595010 M apparatus (open capillary method) and are
782 uncorrected. Nuclear magnetic resonance (NMR) spectra were
783 recorded at 300 MHz on a Varian Mercury 300 instrument at
784 ambient temperature in the specified deuterated solvent. Chemical
785 shifts (δ) are quoted in parts per million (ppm) and are referenced to
786 the residual solvent peak. The coupling constants J are given in hertz
787 (Hz). The following abbreviations were used: s (singlet), d (doublet),
788 t (triplet), dd (doublet of doublet), m (multiplet), brs (broad signal).
789 Signals due to NH/OH protons were located by deuterium exchange
790 with D_2O . Noncommercial 7-hydroxy-3-methylcoumarin,⁴⁵ 7-hydroxy-
791 3,4-dimethylcoumarin,⁴⁴ 7-hydroxy-3-cyanocoumarin,⁸⁰ and 7-hy-
792 droxy-4-(hydroxymethyl)coumarin,³⁵ were prepared as referenced.

793 Analytical data of final compounds **2–40**, **42**, **43**, and **45** are
794 reported in Table 6. Analytical details and spectroscopic data of all the
795 intermediates **1a–k** and final compounds are available as Supporting
796 Information.

797 **General Procedure for the Synthesis of 7-(ω -Bromoalky-
798 loxy)-3,4-dimethylcoumarins **1a–d**, 7-(3-(bromomethyl)-
799 benzyloxy)coumarin **1e**, and 7-(4-(bromomethyl)benzyloxy)-
800 3,4-substituted Coumarins **1f–k**.** A Pyrex vessel was charged with
801 a magnetic stirring bar, and then the appropriate 7-hydroxycoumarin
802 derivative (5.0 mmol) and potassium carbonate (0.70 g, 5.0 mmol)
803 were suspended in dry acetonitrile (20 mL). The suitable
804 commercially available dibromo-derivative (1, ω -dibromoalkane or
805 α,α' -dibromo-*m*-xylene or α,α' -dibromo-*p*-xylene, 25 mmol) was
806 added. The reactor was placed in a microwave apparatus and irradiated
807 at 130 $^\circ\text{C}$ for 30 min. After cooling to room temperature, the solid
808 residue was filtered and washed with dichloromethane. The solution
809 was concentrated to dryness, and the resulting crude was purified
810 through flash chromatography (gradient eluent, different mixtures of
811 ethyl acetate in *n*-hexane).

812 **2-(4-(Bromomethyl)phenyl)ethanol (41a).** (4-Bromomethyl)-
813 phenylacetic acid (0.60 g, 2.6 mmol) was dissolved under magnetic
814 stirring with 8 mL of anhydrous THF in a flame-dried round-bottomed
815 flask kept to 0 $^\circ\text{C}$. Borane-dimethyl sulfide (0.40 mL, 3.9 mmol) was
816 then added dropwise and the mixture carefully cooled to room
817 temperature and then left for additional 2 h. Water was cautiously
818 added, and the organic solvent was evaporated. Aqueous layer was
819 extracted with ethyl acetate; the organic layers were collected, dried
820 over sodium sulfate, and evaporated to dryness to give the title
821 product. Yield: 87%. ^1H NMR (DMSO- d_6) δ : 2.69 (t, $J = 7.1$ Hz, 2H),
822 3.57 (t, $J = 7.1$ Hz, 1H, exch. D_2O), 3.79–3.87 (m, 2H), 4.66 (s, 2H),
823 7.18 (d, $J = 7.7$ Hz, 2H), 7.33 (d, $J = 7.7$ Hz, 2H).

824 **7-[[4-(2-Hydroxyethyl)benzyl]oxy]-2H-chromen-2-one (41b).** A
825 Pyrex vessel was charged with a magnetic stirring bar, and then 7-
826 hydroxycoumarin (0.32 g, 2.0 mmol) and potassium carbonate (0.28 g,
827 2.0 mmol) were suspended in dry acetone (12 mL). Bromide **41a**
828 (0.43 g, 2.0 mmol) was added, and the reactor was placed in a
829 microwave apparatus and irradiated at 130 $^\circ\text{C}$ for 30 min. After
830 cooling to room temperature, the solid residue was filtered and washed
831 with dichloromethane. The solution was concentrated to dryness, and
832 the resulting oil was purified through flash chromatography (gradient
833 eluent, methanol in dichloromethane 0% \rightarrow 10%). Yield: 77%. ^1H
834 NMR (DMSO- d_6) δ : 2.70 (t, $J = 7.1$ Hz, 2H), 3.56–3.61 (m, 2H),
835 4.59–4.63 (m, 1H, exch. D_2O), 5.15 (s, 2H), 6.27 (d, $J = 9.6$ Hz, 1H),
836 6.98–7.06 (m, 2H), 7.35 (d, $J = 8.0$ Hz, 2H), 7.22 (d, $J = 8.0$ Hz, 2H),
837 7.62 (d, $J = 8.5$ Hz, 1H), 7.97 (d, $J = 9.6$ Hz, 1H).

838 **7-(4-(2-Bromoethyl)benzyloxy)-2H-chromen-2-one (41c).** Inter-
839 mediate **41b** (0.40 g, 1.4 mmol) was dissolved in 5.0 mL of anhydrous

dichloromethane under stirring with carbon tetrabromide (0.49 g, 1.5
mmol). To this mixture, a solution of triphenylphosphine (0.43 g, 1.6
mmol) in 5.0 mL of anhydrous dichloromethane was dropped at 0 $^\circ\text{C}$
and the resulting solution was kept at room temperature for 4 h.
Evaporation of the solvent and purification by flash chromatography
(gradient eluent, ethyl acetate in *n*-hexane 0% \rightarrow 60%) afforded
bromide **41c**. Yield: 77% yield. ^1H NMR (DMSO- d_6) δ : 3.12 (t, $J =$
7.1 Hz, 2H), 3.72 (t, $J = 7.1$ Hz, 2H), 5.17 (s, 2H), 6.28 (d, $J = 9.6$ Hz,
1H), 7.00 (dd, $J_1 = 8.5$ Hz, $J_2 = 2.5$ Hz, 1H), 7.06 (d, $J = 2.5$ Hz, 1H),
7.29 (d, $J = 8.0$ Hz, 2H), 7.40 (d, $J = 8.0$ Hz, 2H), 7.62 (d, $J = 8.5$ Hz,
1H), 7.97 (d, $J = 9.6$ Hz, 1H).

850
851 **(2E)-N-(3-Methoxyphenyl)-3-phenylacrylamide (44a).** To a sus-
852 pension of *trans*-cinnamic acid (0.89 g, 6.0 mmol) in dry dichloro-
853 methane (5.0 mL), thionyl chloride (5.0 mL) was added. The resulting
854 reaction mixture was refluxed for 6 h and then concentrated to
855 dryness. The oily residue was dissolved in dry dichloromethane (20
856 mL), and *m*-anisidine (0.67 mL, 6.0 mmol) was slowly added. After
857 refluxing for 4 h, the solvent was evaporated under vacuum and the
858 resulting crude was crystallized from hot ethanol. Yield: 70%. ^1H NMR
(DMSO- d_6) δ : 3.73 (s, 3H), 6.61–6.66 (m, 1H), 6.81 (d, $J = 15.7$ Hz,
859 1H), 7.18–7.25 (m, 2H), 7.36–7.46 (m, 4H), 7.53–7.62 (m, 3H),
860 10.17 (s, 1H, exch. D_2O).

861
862 **7-Hydroxy-2-quinolinone (44b).**⁷⁰ Phenylacrylamide **44a** (0.63 g,
863 2.5 mmol) was dissolved in chlorobenzene (12 mL) in a flame-dried
864 round-bottomed flask. AlCl_3 (1.3 g, 10 mmol) was added portionwise
865 while cooling to 0 $^\circ\text{C}$. The reaction mixture was refluxed for 8 h, then
866 cooled and poured into crushed ice. The resulting precipitate was
867 washed with chloroform followed by diethyl ether, thus yielding the
868 desired intermediate. Yield: 67%. ^1H NMR (DMSO- d_6) δ : 6.19 (d, $J =$
869 9.3 Hz, 1H), 6.59–6.71 (m, 2H), 7.42 (d, $J = 8.3$ Hz, 1H), 7.72 (d, $J =$
870 9.3 Hz, 1H), 10.08 (s, 1H, exch. D_2O), 11.48 (s, 1H, exch. D_2O).

871 **7-(4-(Bromomethyl)benzyloxy)-2H-quinolin-2-one (44c).** In a
872 Pyrex vessel charged with a magnetic and a Weflon stirring bar,
873 phenol **44b** (0.24 g, 1.5 mmol) and potassium carbonate (0.21 g, 1.5
874 mmol) were suspended in dry acetone (10 mL). α,α' -Dibromo-*p*-
875 xylene (1.2 g, 4.5 mmol) was added, and the reactor was placed in a
876 microwave apparatus and irradiated at 130 $^\circ\text{C}$ for 30 min. After
877 cooling to room temperature, the solid residue was filtered off and
878 washed with dichloromethane. The solution was concentrated to
879 dryness, and the resulting crude solid was purified through flash
880 chromatography (gradient eluent, methanol in dichloromethane 0% \rightarrow
881 10%). Yield: 49%. ^1H NMR (DMSO- d_6) δ : 4.71 (s, 2H), 5.13 (s, 2H),
882 6.28 (d, $J = 9.3$ Hz, 1H), 6.84–6.85 (m, 2H), 7.40–7.57 (m, 5H), 7.78
883 (d, $J = 9.3$ Hz, 1H), 11.60 (brs, 1H, exch. D_2O).

884 **General Procedure for the Synthesis of Final Compounds**
885 **2–40**, **42**, **43**, and **45**. Appropriate bromide **1a–k**, **41c**, or **44c** (0.50
886 mmol) were suspended under magnetic stirring in 4.0 mL of
887 anhydrous acetonitrile in a Pyrex microwave reactor in the presence
888 of potassium carbonate (0.64 g, 0.50 mmol) and a catalytic amount of
889 potassium iodide (for compounds **2–12** and **42–43**). Benzylamine
890 (2.5 mmol), suitable substituted *N*-methylbenzylamine^{81,82} (0.75
891 mmol), or *N*-ethylbenzylamine (0.75 mmol) was added. The vessel
892 was placed in a microwave apparatus and heated at 130 $^\circ\text{C}$ for 30 min.
893 After cooling to room temperature, the reaction mixture was poured
894 into ice-cold water (50 g) and extracted with dichloromethane (3 \times 20
895 mL). The organic fractions were collected, dried over anhydrous
896 sodium sulfate, and evaporated to dryness to give a residue that was
897 crystallized from an appropriate solvent (as indicated in the
898 Supporting Information) or purified by flash chromatography
899 (gradient eluent: different mixtures of methanol in dichloromethane
900 or ethyl acetate in *n*-hexane). Compounds **2**, **3**, **7–10**, and **12** were
901 crystallized as hydrochlorides by treatment with HCl 1.25 N in
902 ethanol. Compounds **5**, **14**, **16–18**, **22–37**, **39–40**, **42**, **43**, and **45**
903 were transformed into the corresponding hydrochloride salts by
904 treating the crude oil with HCl 4.0 N in 1,4-dioxane (commercially
905 available) or by dissolving the solid crude in the minimum volume of
906 1,4-dioxane before adding HCl 4.0 N in 1,4-dioxane.

907 **Rat and Human Monoamine Oxidase Inhibition Assays.** 907
908 rMAO inhibitory activity of compounds in Tables 1–3 was assessed
909 using a continuous spectrophotometric assay,⁸³ monitoring the rate of

910 oxidation of the nonselective nonfluorescent MAO substrate kynur-
911 amine to 4-hydroxyquinoline. MAO-A and MAO-B activities in rat
912 mitochondrial preparations were assayed using as the controls the
913 selective and irreversible inhibitors clorgyline (250 nM) and (-)-L-
914 deprenyl (250 nM), respectively. IC₅₀ values were determined by
915 nonlinear regression of MAO inhibition vs -log of the concentration
916 plots, using the program Origin, version 6.0 (Microcal Software Inc.,
917 Northampton, MA).

918 Human monoamine oxidase inhibition assays were carried out with
919 a fluorescence based method,⁷² also using kynuramine as nonselective
920 substrate of MAO-A and MAO-B. Briefly, reactions were performed in
921 triplicate in black, flat-bottomed polystyrene 96-well microtiter plates
922 (FluoroNunc/LumiNunc, MaxiSorp™ surface, NUNC, Roskilde,
923 Denmark) containing potassium phosphate buffer (158 μL), an
924 aqueous stock solution of kynuramine 0.5 mM (final kynuramine
925 concentration corresponding to 50 μM), and DMSO solution of
926 inhibitor in final concentrations ranging from 10⁻⁴ to 10⁻¹¹ M.
927 Samples were incubated at 37 °C, and then diluted human
928 recombinant MAO-A and MAO-B (Supersomes; BD Gentest,
929 Woburn, MA) were delivered to obtain final protein concentrations
930 of 0.009 and 0.015 mg/mL, respectively. Incubation was carried out at
931 37 °C for 30 min, and then the reactions were stopped by addition of
932 75 μL of 2N NaOH.

933 Formation of 4-hydroxyquinoline was quantified with a 96-well
934 microplate fluorescence reader (FLx 800, BioTek Instruments, Inc.
935 Winooski, USA) at excitation/emission wavelengths of 310/400 nm
936 (20 nm slit width for excitation, 30 nm slit width for emission).
937 Inhibitory activities (IC₅₀s) were determined by means of nonlinear
938 regressions performed with GraphPad Prism 5.0 software. Results are
939 the mean of at least two independent experiments.

940 **Electric Eel, Equine Serum, and Human Cholinesterases**
941 **Inhibition Assays.** The spectrophotometric Ellman's test⁷¹ for in
942 vitro inhibition assay of AChE from electric eel (463 U/mg; Sigma)
943 and BChE from equine serum (13 U/mg; Sigma) was followed as
944 previously described.²⁴ The concentration of compound which
945 determined 50% inhibition of the cholinesterase activity (IC₅₀) was
946 calculated by nonlinear regression of the response/log(concentration)
947 curve, using GraphPad Prism version 5. Kinetic studies were
948 performed with the same test conditions, using six concentrations of
949 substrate (from 0.033 to 0.2 mM) and four concentrations of inhibitor
950 (0–0.25 μM). Apparent inhibition constants and kinetic parameters
951 were calculated within the "Enzyme kinetics" module of Prism.
952 Inhibition tests on human recombinant AChE (2770 U/mg; Sigma)
953 and BChE from human serum (50 U/mg; Sigma) were run under the
954 same experimental conditions used for eeAChE.

955 **Bidirectional Transport Studies on MDCKII-MDR1 Mono-**
956 **layers.** MDCKII-MDR1 cells were cultured in DMEM medium and
957 seeded at a density of 100000 cell/cm² onto polyester 12-well
958 Transwell inserts (pore size 0.4 μm, 12 mm diameter, apical volume
959 0.5 mL, basolateral volume 1.5 mL). MDCKII-MDR1 cell barrier
960 function was verified prior to the described transport experiments by
961 means of trans-epithelial electrical resistance (TEER) using an EVOM
962 apparatus, and the measurement of the flux of fluorescein
963 isothiocyanate-dextran (FD4, Sigma-Aldrich, Italy) (200 μg/mL)
964 and diazepam (75 μM). The TEER was measured in growth media
965 (DMEM) at room temperature and calculated as the measured
966 resistance minus the resistance of an empty Transwell (blank without
967 cells). Cell monolayers with TEER values 800 Ohm/cm² were used.
968 Following the TEER measurements, the cells were equilibrated in
969 transport medium in both the apical and basolateral chambers for 30
970 min at 37 °C. The composition of transport medium was as follows:
971 0.4 mM K₂HPO₄, 25 mM NaHCO₃, 3 mM KCl, 122 mM NaCl, and
972 10 mM glucose, pH = 7.4, and osmolarity 300 mOsm as determined
973 by a freeze point based osmometer. At time 0, culture medium was
974 aspirated from both the AP and BL chambers of each insert, and cell
975 monolayers were washed three times (10 min per wash) with
976 Dulbecco's Phosphate Buffered Saline (DPBS) pH = 7.4. Finally, a
977 solution of compound diluted in transport medium was added to the
978 apical or basolateral chamber. For AP-to-BL or BL-to-AP flux studies,
979 the drug solution was added in the AP chamber or in the BL chamber,

respectively. Except for FD4, which was solubilized directly in the
980 assay medium at a concentration of 200 μg/mL, the other compounds
981 were first dissolved in DMSO and then diluted with the assay medium
982 to a final concentration of 75 μM. Next, the tested solutions were
983 added to the donor side (0.5 mL for the AP chamber and 1.5 mL for
984 the BL chamber), and fresh assay medium was placed in the receiver
985 compartment. The percentage of DMSO never exceeded 1% (v/v) in
986 the samples. The transport experiments were carried out under cell
987 culture conditions (37 °C, 5% CO₂, 95% humidity). After incubation
988 time of 120 min, samples were removed from the apical and
989 basolateral side of the monolayer and then stored until further analysis.
990

Quantitative analysis of compounds 37 and diazepam were
991 performed through UV-visible (Vis) spectroscopy using a Perkin-
992 Elmer double-beam UV-visible spectrophotometer Lambda Bio 20
993 (Milan, Italy), equipped with 10 mm path-length-matched quartz cells.
994 Standard calibration curves were prepared at maximum absorption
995 wavelength of each compound using PBS as solvent and were linear (*r*²
996 = 0.999) over the range of tested concentration (from 5 to 100 μM).
997 The FD4 samples were analyzed with a Victor3 fluorimeter (Wallac
998 Victor3, 1420 multilabel counter, PerkinElmer) at excitation and
999 emission wavelengths of 485 and 535 nm, respectively. Each
1000 compound was tested in triplicate, and the experiments were repeated
1001 three times.
1002

The apparent permeability, in units of cm/s, was calculated using
1003 the following equation:
1004

$$P_{app} = \left(\frac{V_A}{\text{area} \times \text{time}} \right) \times \left(\frac{[\text{drug}]_{\text{acceptor}}}{[\text{drug}]_{\text{initial}}} \right)$$

where "V_A" is the volume in the acceptor well, "area" is the surface area
1005 of the membrane, "time" is the total transport time, "[drug]_{acceptor}" is
1006 the concentration of the drug measured by UV-spectroscopy, and
1007 "[drug]_{initial}" is the initial drug concentration in the AP or BL chamber.
1008 Efflux ratio (ER) was calculated using the following equation: ER =
1009 P_{app} BL-AP/P_{app} AP-BL, where P_{app} BL-AP is the apparent
1010 permeability of basal-to-apical transport, and P_{app} AP-BL is the
1011 apparent permeability of apical-to-basal transport. An efflux ratio
1012 greater than 2 indicates that a test compound is likely to be a substrate
1013 for P-gp transport.
1014

Cytotoxicity Assays. Human neuroblastoma cells SH-SY5Y were
1015 maintained at 37 °C in a humidified incubator containing 5% CO₂ in
1016 DMEM nutrient (Lonza) supplemented with 10% heat inactivated
1017 FBS, 2 mM L-glutamine, 100 U/mL penicillin, and 100 μg/mL
1018 streptomycin. Cells were dispensed into 96-well microtiter plates at a
1019 density of 10000 cells/well. Following overnight incubation, cells were
1020 treated with a range of compound concentrations (0.1–50 μM). Then
1021 the plates were incubated at 37 °C for 24, 48, and 72 h. An amount of
1022 10 μL of 0.5% w/v MTT was further added to each well, and the plates
1023 were incubated for an additional 3 h at 37 °C. Finally the cells were
1024 lysed by addition of 100 μL of DMSO/EtOH 1:1 (v/v) solution. The
1025 absorbance at 570 nm was determined using a PerkinElmer 2030
1026 multilabel reader Victor TM X3.
1027

Neuroprotection against Oxidative Stress. Human neuro-
1028 blastoma SH-SY5Y cells were dispensed into 96-well microtiter plates
1029 at a density of 10000 cells/well. Following overnight incubation, cells
1030 were treated with a range of compound concentrations (1 and 10 μM)
1031 at time zero and maintained for 24 h. Then, the media were replaced
1032 by fresh media still containing the drug plus the cytotoxic stimulus
1033 represented by 60 μM H₂O₂ that was left for an additional 24 h period.
1034 Thereafter, cell survival was determined using the 3-(4,5-dimethylth-
1035 iazol-2-yl)-2,5-diphenyl-tetrazolium bromide (MTT) assay. The
1036 putative cytotoxic effects of 37 and of H₂O₂ were studied by exposing
1037 the cells to the compound at the highest concentration used in the
1038 neuroprotection studies for 24 h. Each compound was tested in
1039 triplicate, and the experiments were repeated three times. Statistical
1040 significance was assigned to *p* < 0.01 and calculated using a one-way
1041 analysis of variance (ANOVA) followed by the Bonferroni post hoc
1042 tests (GraphPad Prism vers. 5). Where indicated, standard error of the
1043 mean (SD) for data points has been calculated and the number of
1044 experiments is given (*n*).
1045

Molecular Docking. GOLD (version 5.2), a genetic algorithm-based software, was used for the docking study. ChemPLP was selected as a fitness function. Automatic genetic algorithm parameter settings were used. All the crystal structures used in docking simulations were retrieved from the Protein Data Bank. In particular, the entry codes 1EVE and 4EY7 were downloaded for modeling hAChE and TcAChE, respectively; the entry code 2V60 was downloaded for hMAO-B, whereas a previously built homology modeling was used for rMAO-B.⁴⁷ The Protein Preparation Wizard available from Schroedinger⁸⁴ was used for the protein pretreatment in order to add missing hydrogen atoms, define the protonation states at pH equal to 7.4 and tautomers for histidine residues and to minimize the whole structure. For each simulation, 10 conformations were generated for each inhibitor in a sphere of a 17 Å, using as references the centroids of ligand cocrystallized in 1EVE and 2V60. In MAO docking runs, the X-ray coordinates of 7-(3-chlorobenzoyloxy)-4-carboxaldehyde-coumarin taken from 2V60 were used as a scaffold to constrain bias binding mode toward MAO-B. In addition, the side chains of Glu206, Tyr112, Asn116, and His115 (mutated to Tyr115 in the case of rMAO-B) were set as flexible. Finally, eight ordered water molecules were explicitly taken into account in docking runs, as elsewhere reported.⁶⁸

ASSOCIATED CONTENT

Supporting Information

Analytical and spectroscopic (¹H NMR) data for intermediates **1a–k** and final compounds **2–40**, **42**, **43**, and **45** (PDF); SMILES data (CSV). The Supporting Information is available free of charge on the ACS Publications website at DOI: 10.1021/acs.jmedchem.5b00599.

AUTHOR INFORMATION

Corresponding Authors

*Marco Catto: phone, +39 080 5442803; fax, +39 080 5442230; E-mail, marco.catto@uniba.it.

*Angelo Carotti: phone, +39 080 5442782; fax, +39 080 5442230; E-mail, angelo.carotti@uniba.it

Present Address

¹⁰⁸²Ensemble Therapeutics, 99 Erie Street, Cambridge Massachusetts 02139, United States.

Author Contributions

All authors contributed to the writing of the manuscript, gave approval to the final version of the manuscript and declared no conflict of interest.

Notes

The authors declare no competing financial interest.

ACKNOWLEDGMENTS

WE thank MIUR (Rome, Italy) for partial financial support.

ABBREVIATIONS USED

3D-QSAR, three-dimensional quantitative structure–activity relationships; A β , beta amyloid protein; ACh, acetylcholine; AChE, acetylcholinesterase; AChEI, AChE inhibitors; AD, Alzheimer's disease; BBB, blood–brain barrier; BChE, butyrylcholinesterase; CAS, catalytic anionic binding site; DBS, dual binding site; DMEM, Dulbecco's Modified Eagle Medium; ER, efflux ratio; ESI-MS, electrospray ionization mass spectrometry; FAD, flavin adenine dinucleotide; FD4, fluorescein isothiocyanate-dextran; MAO-A, monoamine oxidase A; MAO-B, monoamine oxidase B; MTT, 3-(4,5-dimethylthiazol-2-yl)-2,5-diphenyltetrazolium bromide; ND, neurodegenerative disease; NMDA, N-methyl-D-aspartate; P_{app}, apparent permeability; P_{app} AP-BL, apparent permeability

apical-to-basal; P_{app} BL-AP, apparent permeability basal-to-apical; PAS, peripheral anionic binding site; PD, Parkinson's disease; P-gp, P-glycoprotein; ROS, reactive oxygen species; SAR, structure–activity relationships; SSR, structure–selectivity relationships; TEER, trans-epithelial electrical resistance

REFERENCES

- (1) (a) Banerjee, S. The Macroeconomics of Dementia—Will the World Economy get Alzheimer's Disease? *Arch. Med. Res.* **2012**, *43*, 705–709. (b) Narayan, P.; Ehsani, S.; Lindquist, S. Combating Neurodegenerative Disease with Chemical Probes and Model Systems. *Nature Chem. Biol.* **2014**, *10*, 911–920.
- (2) Trippier, P. C.; Labby, K. J.; Hawker, D. D.; Mataka, J. J.; Silverman, R. B. Target- and Mechanism-Based Therapeutics for Neurodegenerative Diseases: Strength in Numbers. *J. Med. Chem.* **2013**, *56*, 3121–3147.
- (3) Alzheimer's Association. 2015 Alzheimer's disease facts and figures. *Alzheimer's Dementia* **2015**, *11*, 332–384.
- (4) Misra, S.; Medhi, B. Drug Development Status for Alzheimer's Disease: Present Scenario. *Neurol. Sci.* **2013**, *34*, 831–839.
- (5) Berk, C.; Sabbagh, M. N. Successes and Failures for Drugs in Late-Stage Development for Alzheimer's Disease. *Drugs Aging* **2013**, *10*, 783–792.
- (6) Querfurth, H. W.; LaFerla, F. M. Alzheimer's Disease. *N. Engl. J. Med.* **2010**, *362*, 329–344.
- (7) Chakrabarti, S.; Sinha, M.; Thakurta, I. G.; Banerjee, P.; Chattopadhyay, M. Oxidative Stress and Amyloid Beta Toxicity in Alzheimer's Disease: Intervention in a Complex Relationship by Antioxidants. *Curr. Med. Chem.* **2013**, *20*, 4648–4664.
- (8) Terry, A. V.; Buccafusco, J. J. The Cholinergic Hypothesis of Age and Alzheimer's Disease-Related Cognitive Deficits: Recent Challenges and Their Implications for Novel Drug Development. *J. Pharmacol. Exp. Ther.* **2003**, *306*, 821–827.
- (9) Anand, P.; Singh, B. A Review on Cholinesterase Inhibitors for Alzheimer's Disease. *Arch. Pharm. Res.* **2013**, *36*, 375–399.
- (10) Cheewakriengkrai, L.; Gauthier, S. A 10-Year Perspective on Donepezil. *Expert Opin. Pharmacother.* **2013**, *14*, 331–338.
- (11) Lo, D.; Grossberg, G. T. Use of Memantine for the Treatment of Dementia. *Expert Rev. Neurother.* **2011**, *11*, 1359–1370.
- (12) Darvesh, S.; Hopkins, D. A.; Geula, C. Neurobiology of Butyrylcholinesterase. *Nature Rev. Neurosci.* **2003**, *2*, 131–138.
- (13) Harel, M.; Schalk, I.; Ehret-Sabatier, L.; Bouet, F.; Goeldner, M.; Hirth, C.; Axelsen, P. H.; Silman, I.; Sussman, J. L. Quaternary Ligand Binding to Aromatic Residues in the Active-Site Gorge of Acetylcholinesterase. *Proc. Natl. Acad. Sci. U. S. A.* **1993**, *90*, 9031–9035.
- (14) Kryger, G.; Silman, I.; Sussman, J. L. Structure of Acetylcholinesterase Complexed with E2020 (Aricept): Implications for the Design of New Anti-Alzheimer Drugs. *Structure* **1999**, *7*, 297–307.
- (15) Tarozzi, A.; Bartolini, M.; Piazzini, L.; Valgimigli, L.; Amorati, R.; Bolondi, C.; Djemil, A.; Mancini, F.; Andrisano, V.; Rampa, A. From the Dual Function Lead AP2238 to AP2469, a Multi-Target-Directed Ligand for the Treatment of Alzheimer's Disease. *Pharmacol. Res. Perspect.* **2014**, *2*, e00023.
- (16) Dvira, H.; Silman, I.; Harel, M.; Rosenberry, T. L.; Sussman, J. L. Acetylcholinesterase: From 3D Structure to Function. *Chem. Biol. Interact.* **2010**, *187*, 10–22.
- (17) Pisani, L.; Catto, M.; Giangreco, I.; Leonetti, F.; Nicolotti, O.; Stefanachi, A.; Cellamare, S.; Carotti, A. Design, Synthesis and Biological Evaluation of Coumarin Derivatives Tethered to an Edrophonium-like Fragment as Highly Potent and Selective Dual Binding Site Acetylcholinesterase Inhibitors. *ChemMedChem* **2010**, *5*, 1616–1630.
- (18) Catto, M.; Pisani, L.; Leonetti, F.; Nicolotti, O.; Pesce, P.; Stefanachi, A.; Cellamare, S.; Carotti, A. Design, Synthesis and Biological Evaluation of Coumarin Alkylamines as Potent and Selective

- 1172 Dual Binding Site Inhibitors of Acetylcholinesterase. *Bioorg. Med. Chem.* **2013**, *21*, 146–152.
- 1174 (19) Leonetti, F.; Catto, M.; Nicolotti, O.; Pisani, L.; Cappa, A.; Stefanachi, A.; Carotti, A. Homo- and Heterobivalent Edrophonium-like Ammonium Salts as Highly Potent, Dual Binding Site AChE Inhibitors. *Bioorg. Med. Chem.* **2008**, *16*, 7450–7456.
- 1178 (20) Conejo-Garcia, A.; Pisani, L.; del Carmen Nunez, M.; Catto, M.; Nicolotti, O.; Leonetti, F.; Campos, J. M.; Gallo, M. A.; Espinosa, A.; Carotti, A. Homodimeric Bis-Quaternary Heterocyclic Ammonium Salts as Potent Acetyl- and Butyrylcholinesterase Inhibitors: A Systematic Investigation of the Influence of Linker and Cationic Heads over Affinity and Selectivity. *J. Med. Chem.* **2011**, *54*, 2627–2645.
- 1185 (21) Nicolotti, O.; Pisani, L.; Catto, M.; Leonetti, F.; Giangreco, I.; Stefanachi, A.; Carotti, A. Discovery of a Potent and Selective Heterobivalent AChE Inhibitor via Bioisosteric Replacement. *Mol. Inform.* **2011**, *30*, 133–136.
- 1189 (22) Carotti, A.; De Candia, M.; Catto, M.; Borisova, T. N.; Varlamov, A. V.; Mendez-Alvarez, E.; Soto-Otero, R.; Voskressensky, L. G.; Altomare, C. Ester Derivatives of Annulated Tetrahydrozocines: A New Class of Selective Acetylcholinesterase Inhibitors. *Bioorg. Med. Chem.* **2006**, *14*, 7205–7212.
- 1194 (23) Tasso, B.; Catto, M.; Nicolotti, O.; Novelli, F.; Tonelli, M.; Giangreco, I.; Pisani, L.; Sparatore, A.; Boido, V.; Carotti, A.; Sparatore, F. Quinolizidinyl Derivatives of Bi- and Tricyclic Systems as Potent Inhibitors of Acetyl- and Butyrylcholinesterase with Potential in Alzheimer's Disease. *Eur. J. Med. Chem.* **2011**, *46*, 2170–2184.
- 1200 (24) Catto, M.; Berezin, A. A.; Lo Re, D.; Loizou, G.; Demetriades, M.; De Stradis, A.; Campagna, F.; Koutentis, P. A.; Carotti, A. Design, Synthesis and Biological Evaluation of Benzo[e][1,2,4]triazin-7(1H)-one and [1,2,4]-Triazino[5,6,1-jk]carbazol-6-one Derivatives as Dual Inhibitors of Beta-Amyloid Aggregation and Acetyl/Butyryl Cholinesterase. *Eur. J. Med. Chem.* **2012**, *58*, 84–97.
- 1206 (25) Youdim, M. B.; Edmondson, D.; Tipton, K. F. The Therapeutic Potential of Monoamine Oxidase Inhibitors. *Nature Rev. Neurosci.* **2006**, *7*, 295–309.
- 1209 (26) Edmondson, D. E.; Mattevi, A.; Binda, C.; Li, M.; Hubalek, F. Structure and Mechanism of Monoamine Oxidases. *Curr. Med. Chem.* **2004**, *11*, 1983–1993.
- 1212 (27) Grimsby, J.; Lan, N. C.; Neve, R.; Chen, K.; Shih, J. C. Tissue Distribution of Human Monoamine Oxidase-A and Oxidase-B Messenger-RNA. *J. Neurochem.* **1990**, *55*, 1166–1169.
- 1215 (28) Fowler, C. J.; Ross, S. B. Selective Inhibitors of Monoamine Oxidase A and B: Biochemical, Pharmacological, and Clinical Properties. *Med. Res. Rev.* **1984**, *4*, 323–358.
- 1218 (29) Pisani, L.; Catto, M.; Leonetti, F.; Nicolotti, O.; Stefanachi, A.; Campagna, F.; Carotti, A. Targeting Monoamine Oxidases with Multipotent Ligands: An Emerging Strategy in the Search of New Drugs Against Neurodegenerative Diseases. *Curr. Med. Chem.* **2011**, *18*, 4568–4587.
- 1223 (30) Salat, D.; Tolosa, E. Levodopa in the Treatment of Parkinson's Disease: Current Status and New Developments. *J. Parkinson's Dis.* **2013**, *3*, 255–269.
- 1226 (31) De Colibus, L.; Li, M.; Binda, C.; Lustig, A.; Edmondson, D. E.; Mattevi, A. Three-Dimensional Structure of Human Monoamine Oxidase A (MAO-A): Relation to the Structures of Rat MAO-A and Human MAO-B. *Proc. Natl. Acad. Sci. U. S. A.* **2005**, *102*, 12684–12689.
- 1231 (32) Son, S.-Y.; Ma, J.; Kondou, Y.; Yoshimura, M.; Yamashita, E.; Tsukahara, T. Structure of Human Monoamine Oxidase A at 2.2-Å Resolution: The Control of Opening the Entry for Substrates/Inhibitors. *Proc. Natl. Acad. Sci. U. S. A.* **2008**, *105*, S739–S744.
- 1235 (33) Binda, C.; Newton-Vinson, P.; Hubalek, F.; Edmondson, D. E.; Mattevi, A. Structure of Human Monoamine Oxidase B, a Drug Target for the Treatment of Neurological Disorders. *Nature Struct. Mol. Biol.* **2002**, *9*, 22–26.
- 1239 (34) Binda, C.; Hubalek, F.; Li, M.; Herzig, Y.; Sterling, J.; Edmondson, D. E.; Mattevi, A. Crystal Structures of Monoamine Oxidase B in Complex with Four Inhibitors of the N-Propargylaminoindan Class. *J. Med. Chem.* **2004**, *47*, 1767–1774.
- (35) Binda, C.; Wang, J.; Pisani, L.; Caccia, C.; Carotti, A.; Salvati, P.; Edmondson, D. E.; Mattevi, A. Structures of Human Monoamine Oxidase B Complexes with Selective Noncovalent Inhibitors: Safinamide and Coumarin Analogs. *J. Med. Chem.* **2007**, *50*, 5848–5852.
- (36) Riederer, P.; Danielczyk, W.; Gruenblatt, E. Monoamine Oxidase-B Inhibition in Alzheimer's Disease. *Neurotoxicology* **2004**, *1–2*, 271–277.
- (37) Qureshi, I. A.; Mehler, M. F. Advances in Epigenetics and Epigenomics for Neurodegenerative Diseases. *Curr. Neurol. Neurosci. Rep.* **2011**, *11*, 464–473.
- (38) Leon, R.; Garcia, A. G.; Marco-Contelles, J. Recent Advances in the Multitarget-Directed Ligands Approach for the Treatment of Alzheimer's Disease. *Med. Res. Rev.* **2013**, *33*, 139–189.
- (39) Morphy, J. R.; Harris, C. J. *Designing Multi-Target Drugs*; RSC Publishing: London, 2012.
- (40) Youdim, M. B.; Buccafusco, J. J. CNS Targets for Multifunctional Drugs in the Treatment of Alzheimer's and Parkinson's Diseases. *J. Neural Transm.* **2005**, *112*, 519–537.
- (41) Buccafusco, J. J.; Terry, A. V., Jr. Multiple Central Nervous System Targets for Eliciting Beneficial Effects on Memory and Cognition. *J. Pharmacol. Exp. Ther.* **2000**, *295*, 438–446.
- (42) Nicolotti, O.; Giangreco, I.; Introcaso, A.; Leonetti, F.; Stefanachi, A.; Carotti, A. Strategies of Multi-Objective Optimization in Drug Discovery and Development. *Expert Opin. Drug Discovery* **2011**, *6*, 871–884.
- (43) Kneubuehler, S.; Thull, U.; Altomare, C.; Carta, V.; Gaillard, P.; Carrupt, P. A.; Carotti, A.; Testa, B. Inhibition of Monoamine Oxidase-B by 5H-Indeno[1,2-c]pyridazines: Biological Activities, Quantitative Structure–Activity Relationships (QSARs) and 3DQSARs. *J. Med. Chem.* **1995**, *38*, 3874–3883.
- (44) Gnerre, C.; Catto, M.; Leonetti, F.; Weber, P.; Carrupt, P.-A.; Altomare, C.; Carotti, A.; Testa, B. Inhibition of Monoamine Oxidases by Functionalized Coumarin Derivatives: Biological Activities, QSARs, and 3D-QSARs. *J. Med. Chem.* **2000**, *43*, 4747–4758.
- (45) Catto, M.; Nicolotti, O.; Leonetti, F.; Carotti, A.; Favia, A. D.; Soto-Otero, R.; Mendez-Alvarez, E.; Carotti, A. Structural Insights into Monoamine Oxidase Inhibitory Potency and Selectivity of 7-Substituted Coumarins from Ligand- and Target-Based Approaches. *J. Med. Chem.* **2006**, *49*, 4912–4925.
- (46) Carotti, A.; Melloni, P.; Thaler, F.; Caccia, C.; Maestroni, S.; Salvati, P. Substituted Aminoalkyl and Amidoalkyl Benzopyran Derivatives. WO 2006/102958 A1, 2006.
- (47) Carotti, A.; Catto, M.; Leonetti, F.; Campagna, F.; Soto-Otero, R.; Mendez-Alvarez, E.; Thull, U.; Testa, B.; Altomare, C. Synthesis and Monoamine Oxidase Inhibitory Activity of New Pyridazine-, Pyrimidine-, and 1,2,4-Triazine-Containing Tricyclic Derivatives. *J. Med. Chem.* **2007**, *50*, 5364–5371.
- (48) Leonetti, F.; Capaldi, C.; Pisani, L.; Nicolotti, O.; Muncipinto, G.; Stefanachi, A.; Cellamare, S.; Caccia, C.; Carotti, A. Solid-Phase Synthesis and Insights into Structure–Activity Relationships of Safinamide Analogues as Potent and Selective Inhibitors of Type B Monoamine Oxidase. *J. Med. Chem.* **2007**, *50*, 4909–4916.
- (49) Pisani, L.; Muncipinto, G.; Miscioscia, T. F.; Nicolotti, O.; Leonetti, F.; Catto, M.; Caccia, C.; Salvati, P.; Soto-Otero, R.; Mendez-Alvarez, E.; Passeleu, C.; Carotti, A. Discovery of a Novel Class of Potent Coumarin Monoamine Oxidase B Inhibitors: Development and Biopharmacological Profiling of 7-[(3-Chlorobenzyl)oxy]-4-[(methylamino)methyl]-2H-chromen-2-one Methanesulfonate (NW-1772) as a Highly Potent, Selective, Reversible, and Orally Active Monoamine Oxidase B Inhibitor. *J. Med. Chem.* **2009**, *52*, 6685–6706.
- (50) Pisani, L.; Barletta, M.; Soto-Otero, R.; Nicolotti, O.; Mendez-Alvarez, E.; Catto, M.; Introcaso, A.; Stefanachi, A.; Cellamare, S.; Altomare, C.; Carotti, A. Discovery, Biological Evaluation, and Structure–Activity and –Selectivity Relationships of 6'-Substituted (E)-2-(Benzofuran-3(2H)-ylidene)-N-methylacetamides, a Novel

- 1309 Class of Potent and Selective Monoamine Oxidase Inhibitors. *J. Med.*
1310 *Chem.* **2013**, *56*, 2651–2664.
- 1311 (51) Bruehlmann, C.; Ooms, F.; Carrupt, P. A.; Testa, B.; Catto, M.;
1312 Leonetti, F.; Altomare, C.; Carotti, A. Coumarin Derivatives as Dual
1313 Inhibitors of Acetylcholinesterase and Monoamine Oxidase. *J. Med.*
1314 *Chem.* **2001**, *44*, 3195–3198.
- 1315 (52) Carotti, A. *MAOs Long March: From Toxic First-Generation*
1316 *Drugs to Isoform-Selective, Reversible and Multi-Target Inhibitors.*
1317 *Frontiers in CNS and Oncology Medicinal Chemistry*, ACS-EFMC,
1318 Siena, Italy, October 7–9, 2007, COMC-059; American Chemical
1319 Society, Division of Medicinal Chemistry, Washington DC, 2007,
1320 CODEN: 69KAR2.
- 1321 (53) Sterling, J.; Herzig, Y.; Goren, T.; Finkelstein, N.; Lerner, D.;
1322 Goldenberg, W.; Miskolczi, I.; Molnar, S.; Rantal, F.; Tamas, T.; Toth,
1323 G.; Zagyva, A.; Zekany, A.; Lavian, G.; Gross, A.; Friedman, R.; Razin,
1324 M.; Huang, W.; Kraus, B.; Chorev, M.; Youdim, M. B. H.; Weinstock,
1325 M. Novel Dual Inhibitors of AChE and MAO Derived from Hydroxy
1326 Aminoindan and Phenethylamine as Potential Treatment for
1327 Alzheimer's Disease. *J. Med. Chem.* **2002**, *45*, S260–S279.
- 1328 (54) Samadi, A.; de los Ríos, C.; Bolea, I.; Chioua, M.; Iriepa, I.;
1329 Moraleda, I.; Bartolini, M.; Andrisano, V.; Gálvez, E.; Valderas, C.;
1330 Unzeta, M.; Marco-Contelles, J. Multipotent MAO and Cholinesterase
1331 Inhibitors for the Treatment of Alzheimer's Disease: Synthesis,
1332 Pharmacological Analysis and Molecular Modeling of Heterocyclic
1333 Substituted Alkyl and Cycloalkyl Propargyl Amine. *Eur. J. Med. Chem.*
1334 **2012**, *52*, 251–262.
- 1335 (55) Yanez, M.; Vina, D. Dual Inhibitors of Monoamine Oxidase and
1336 Cholinesterase for the Treatment of Alzheimer Disease. *Curr. Top.*
1337 *Med. Chem.* **2013**, *13*, 1692–1706.
- 1338 (56) Passos, C. S.; Simões-Pires, C. A.; Nurisso, A.; Soldi, T. C.;
1339 Kato, L.; de Oliveira, C. M.; de Faria, E. O.; Marcourt, L.; Gottfried,
1340 C.; Carrupt, P.-A.; Henriques, A. T. Indole Alkaloids of Psychotria as
1341 Multifunctional Cholinesterases and Monoamine Oxidases Inhibitors.
1342 *Phytochemistry* **2013**, *86*, 8–20.
- 1343 (57) Zheng, H.; Amit, T.; Bar-Am, O.; Fridkin, M.; Youdim, M. B.
1344 H.; Mandel, S. A. From Anti-Parkinson's Drug Rasagiline to Novel
1345 Multitarget Iron Chelators with Acetylcholinesterase and Monoamine
1346 Oxidase Inhibitory and Neuroprotective Properties for Alzheimer's
1347 Disease. *J. Alzheimer's Dis.* **2012**, *30*, 1–16.
- 1348 (58) Bolea, I.; Gella, A.; Monjas, L.; Perez, C.; Rodriguez-Franco, M.
1349 I.; Marco-Contelles, J.; Samadi, A.; Unzeta, M. Multipotent, Permeable
1350 Drug ASS234 Inhibits $A\beta$ Aggregation, Possesses Antioxidant
1351 Properties and Protects from $A\beta$ -induced Apoptosis In Vitro. *Curr.*
1352 *Alzheimer Res.* **2013**, *10*, 797–808.
- 1353 (59) Bautista-Aguilera, O. M.; Esteban, G.; Chioua, M.; Nikolic, K.;
1354 Agbaba, D.; Moraleda, I.; Iriepa, I.; Soriano, E.; Samadi, A.; Unzeta,
1355 M.; Marco-Contelles, J. Multipotent Cholinesterase/Monoamine
1356 Oxidase Inhibitors for the Treatment of Alzheimer's Disease: Design,
1357 Synthesis, Biochemical Evaluation, ADMET, Molecular Modeling, and
1358 QSAR Analysis of Novel Donepezil–Pyridyl Hybrids. *Drug Des. Devel.*
1359 *Ther.* **2014**, *8*, 1893–1910.
- 1360 (60) Avramovich-Tirosh, Y.; Amit, T.; Bar-Am, O.; Zheng, H.;
1361 Fridkin, M.; Youdim, M. B. H. Therapeutic Targets and Potential of
1362 the Novel Brain Permeable Multifunctional Iron Chelator–Mono-
1363 amine Oxidase Inhibitor Drug, M-30, for the Treatment of Alzheimer's
1364 Disease. *J. Neurochem.* **2007**, *100*, 490–502.
- 1365 (61) Matos, M. J.; Pérez-Cruz, F.; Vazquez-Rodriguez, S.; Uriarte, E.;
1366 Santana, L.; Borges, F.; Olea-Azar, C. Remarkable Antioxidant
1367 Properties of a Series of Hydroxy-3-arylcoumarins. *Bioorg. Med.*
1368 *Chem.* **2013**, *21*, 3900–3906.
- 1369 (62) Li, R. S.; Wang, X. B.; Hu, X. J.; Kong, L. Y. Design, Synthesis
1370 and Evaluation of Flavonoid Derivatives as Potential Multifunctional
1371 Acetylcholinesterase Inhibitors Against Alzheimer's disease. *Bioorg.*
1372 *Med. Chem. Lett.* **2013**, *23*, 2636–2641.
- 1373 (63) Huang, L.; Lu, C.; Sun, Y.; Mao, F.; Luo, Z.; Su, T.; Jiang, H.;
1374 Shan, W.; Li, X. Multitarget-Directed Benzylideneindanone Deriva-
1375 tives: Anti- β -Amyloid ($A\beta$) Aggregation, Antioxidant, Metal Chelation,
1376 and Monoamine Oxidase B (MAO-B) Inhibition Properties against
1377 Alzheimer's Disease. *J. Med. Chem.* **2012**, *55*, 8483–8492.
- (64) Youdim, M. B. H.; Weinstock, M. Molecular Basis of
Neuroprotective Activities of Rasagiline and the anti Alzheimer
Drug, TV3326, [(N-Propargyl-(3R)-aminoindan-5-yl)-ethyl Methyl
Carbamate]. *Cell. Mol. Neurobiol.* **2002**, *21*, S55–S73.
- (65) Anderson, M. C.; Hasan, F.; McCrodden, J. M.; Tipton, K. F.
Monoamine Oxidase Inhibitors and the Cheese Effect. *Neurochem. Res.*
1993, *18*, 1145–1149.
- (66) Macdonald, I. R.; Rockwood, K.; Martin, E.; Darvesh, S.
Cholinesterase Inhibition in Alzheimer's Disease: Is Specificity the
Answer? *J. Alzheimer's Dis.* **2014**, *42*, 379–384.
- (67) Greig, N. H.; Utsuki, T.; Yu, Q.-S.; Zhu, X.; Holloway, H. W.;
Perry, T. A.; Lee, B.; Ingram, D. H.; Lahiri, D. K. A New Therapeutic
Target in AD Treatment: Attention to Butyrylcholinesterase. *Curr.*
Med. Res. Opin. **2001**, *17*, 159–165.
- (68) Pisani, L.; Catto, M.; Nicolotti, O.; Grossi, G.; Di Braccio, M.;
Soto-Otero, R.; Mendez-Alvarez, E.; Stefanachi, A.; Gadaleta, D.;
Carotti, A. Fine Molecular Tuning at Position 4 of 2H-Chromen-2-one
Derivatives in the Search of Potent and Selective Monoamine Oxidase
B Inhibitors. *Eur. J. Med. Chem.* **2013**, *70*, 723–739.
- (69) Pisani, L.; Farina, R.; Nicolotti, O.; Gadaleta, D.; Soto-Otero, R.;
Catto, M.; Di Braccio, M.; Mendez-Alvarez, E.; Carotti, A. In Silico
Design of Novel 2H-Chromen-2-one Derivatives as Potent and
Selective MAO-B Inhibitors. *Eur. J. Med. Chem.* **2015**, *89*, 98–105.
- (70) Wang, T.-C.; Chen, Y.-L.; Lee, K.-H.; Tzeng, C.-C. Lewis Acid
Catalyzed Reaction of Cinnamanilides: Competition of Intramolecular
and Intermolecular Friedel–Crafts Reaction. *Synthesis* **1997**, *9*, 87–90.
- (71) Ellman, G. L.; Courtney, K. D.; Andres, V., Jr.; Feartherstone, R.
M. A New and Rapid Colorimetric Determination of Acetylcholin-
esterase Activity. *Biochem. Pharmacol.* **1961**, *7*, 88–95.
- (72) Novaroli, L.; Daina, A.; Favre, E.; Bravo, J.; Carotti, A.; Leonetti,
F.; Catto, M.; Carrupt, P.-A.; Reist, M. Impact of Species-Dependent
Differences on Screening, Design, and Development of MAO-B
Inhibitors. *J. Med. Chem.* **2006**, *49*, 6264–6272.
- (73) Denizot, F.; Lang, R. Rapid Colorimetric Assay for Cell Growth
and Survival. Modifications to the Tetrazolium Dye Procedure Giving
Improved Sensitivity and Reliability. *J. Immunol. Methods* **1986**, *89*,
271–277.
- (74) Verdonk, M. L.; Cole, J. C.; Hartshorn, M. J.; Murray, C. W.;
Taylor, R. D. Improved Protein–Ligand Docking Using GOLD.
Proteins **2003**, *52*, 609–623.
- (75) Liao, S.-M.; Du, Q.-S.; Meng, J.-Z.; Pang, Z.-W.; Huang, R.-B.
The Multiple Roles of Histidine in Protein Interactions. *Chem. Cent. J.*
2013, *7*, 44.
- (76) Denora, N.; Laquintana, V.; Trapani, A.; Lopodota, A.; Latrofa,
A.; Gallo, J. M.; Trapani, G. Translocator Protein (TSPO) Ligand–
Ara-C (Cytarabine) Conjugates as a Strategy to Deliver Antineoplastic
Drugs and to Enhance Drug Clinical Potential. *Mol. Pharmaceutics*
2010, *7*, 2255–2269.
- (77) Inestrosa, N. C.; Alvarez, A.; Pérez, C. A.; Moreno, R. D.;
Vicente, M.; Linker, C.; Casanueva, O. I.; Soto, C.; Garrido, J.
Acetylcholinesterase Accelerates Assembly of Amyloid-Beta-Peptides
into Alzheimer's Fibrils: Possible Role of the Peripheral Site of the
Enzyme. *Neuron* **1996**, *16*, 881–891.
- (78) Galdeano, C.; Viayna, E.; Arroyo, P.; Bidon-Chanal, A.; Blas, J.
R.; Muñoz-Torrero, D.; Luque, F. J. Structural Determinants of the
Multifunctional Profile of Dual Binding Site Acetylcholinesterase
Inhibitors as Anti-Alzheimer Agents. *Curr. Pharm. Des.* **2010**, *16*,
2818–2836.
- (79) Denora, N.; Cassano, T.; Laquintana, V.; Lopalco, A.; Trapani,
A.; Cimmino, C. S.; Laconca, L.; Giuffrida, A.; Trapani, G. Novel
Codrugs with GABAergic Activity for Dopamine Delivery in the Brain.
Int. J. Pharm. **2012**, *437*, 221–231.
- (80) Fringuelli, F.; Piermatti, O.; Pizzo, F. One-pot Synthesis of 3-
Carboxycoumarins via Consecutive Knoevenagel–Pinner Reactions in
Water. *Synthesis* **2003**, *15*, 2331–2334.
- (81) Piazzini, L.; Belluti, F.; Bisi, A.; Gobbi, S.; Rizzo, S.; Bartolini, M.;
Andrisano, V.; Recanatini, M.; Rampa, A. Cholinesterase inhibitors:
SAR and Enzyme Inhibitory Activity of 3-[ω -(Benzylmethylamino)-
alkoxy]xanthen-9-ones. *Bioorg. Med. Chem.* **2007**, *15*, 575–585.

- 1447 (82) Kumpaty, H. J.; Williamson, J. S.; Bhattacharyya, S. Synthesis of
1448 *N*-Methyl Secondary Amines. *Synth. Commun.* **2003**, *33*, 1411–1416.
- 1449 (83) Mendez-Alvarez, E.; Soto-Otero, R.; Sanchez-Sellero, I.; Lopez-
1450 Rivadulla, L. M.; Lamas, M. Inhibition of Brain Monoamine Oxidase
1451 by Adducts of 1,2,3,4-Tetrahydroisoquinoline with Components of
1452 Cigarette Smoke. *Life Sci.* **1997**, *60*, 1719–1727.
- 1453 (84) Sastry, G. M.; Adzhigirey, M.; Day, T.; Annabhimoju, R.;
1454 Sherman, W. Protein and Ligand Preparation: Parameters, Protocols,
1455 and Influence on Virtual Screening Enrichments. *J. Comput.- Aided*
1456 *Mol. Des.* **2013**, *27*, 221–234.